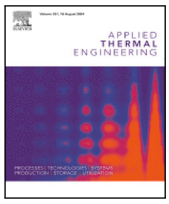
Applied Thermal Engineering 278 (2025) 126926



Contents lists available at ScienceDirect

Applied Thermal Engineering

journal homepage: www.elsevier.com/locate/ate



Research Paper

Multi-objective model predictive control for air-source heat pumps: Leveraging system flexibility to simultaneously reduce noise and increase efficiency

Jonas Klingebiel[1], Moritz Beckschulte[*,1], Florian Will, Christian Vering, Dirk Müller

RWTH Aachen University, E.ON Energy Research Center, Institute for Energy Efficient Buildings and Indoor Climate, Mathieustraße 10, Aachen, 52074, Germany

ARTICLE INFO

Keywords:
Heat pump controller
Flexibility
Control optimization
Sound emission

ABSTRACT

Air-source heat pumps (ASHPs) are pivotal to Europe's transition to decarbonized residential heating. To expand their market reach, improving energy efficiency and reducing noise emissions are essential. Both factors are largely influenced by the compressor and fan speeds, which are managed by the heat pump controller. While advanced control algorithms, such as model predictive control (MPC), have shown promise in enhancing energy efficiency by leveraging system flexibility, their potential for reducing noise emissions remains largely unexplored. This paper presents a multi-objective data-driven MPC using a weighted cost function approach that concurrently improves energy efficiency and reduces noise emissions. We employ a building energy system simulation with an energetically and acoustically calibrated heat pump model and evaluate two MPC strategies: one optimizes efficiency and the other prioritizes noise reduction. We evaluate the robustness of the MPC configurations across two placement scenarios, that introduce variations in noise immission. Compared to a reference controller, the Efficiency-MPC achieves a 10 % $SCOP$ improvement throughout a heating season while reducing acoustic discomfort by up to 20 %. The Acoustic-MPC increases energy efficiency by up to 6 % and significantly reduces acoustic discomfort by up to 92 %. The Acoustic-MPC leverages system flexibility by shifting noise emissions to daytime periods, where higher acoustic limits are allowed. Further, our results show that the MPC's cost function weights remain stable despite changes in heat pump placement. Retuning the weights for the second placement scenario reduces acoustic discomfort by 4 %, suggesting that the MPC configurations can be applied effectively to different scenarios without requiring further adjustments. These results underscore data-driven MPC as a promising tool for optimizing ASHP operation in terms of both efficiency and acoustics.

1. Introduction

In Europe's energy transition, heat pumps represent a promising technology for replacing conventional heating systems [1]. Heat sources of heat pumps include geothermal energy, groundwater, and ambient air. Among these, air source heat pumps (ASHPs) are widely installed in single-family and multi-family buildings due to their relatively low investment costs and the simplicity of planning, installation, and maintenance compared to alternative heat sources [2,3]. As a result, ASHPs accounted for 83% of the heat pump market sales in Europe in 2022 [1]. To harness air as a heat source, ASHPs utilize a finned heat exchanger as an evaporator, which requires a fan to ensure sufficient heat transfer. A growing concern with ASHPs is their noise emissions [4,5], which are primarily generated by the fan and compressor [6]. Meeting noise protection regulations is increasingly challenging, particularly in urban areas with densely packed housing on small plots [7,8]. Research shows that high noise levels from heat pumps can significantly disrupt residents' lives and work, underscoring the need for effective noise reduction measures [6,9,10]. Consequently, reducing ASHP noise emissions holds substantial potential for improving user comfort and enhancing public acceptance of the technology. The literature identifies two main strategies for addressing this issue: design optimization and control optimization.

Regarding **design optimization**, noise-reduced components are being developed. In addressing the noise induced by the fan, researchers are investigating the influence of tip clearance [11] and fan geometry [12]. Further, several studies have examined the interaction between fan and evaporator in relation to noise emission [13–16]. For example, Czwielong and Becker [14] found that larger refrigerant tube

* Corresponding author.
E-mail address: moritz.beckschulte@eonerc.rwth-aachen.de (M. Beckschulte).
[1] These authors contributed equally to this work as co-first authors.

https://doi.org/10.1016/j.applthermaleng.2025.126926
Received 29 November 2024; Received in revised form 10 April 2025; Accepted 21 May 2025
Available online 7 June 2025
1359-4311/© 2025 The Authors. Published by Elsevier Ltd. This is an open access article under the CC BY license (http://creativecommons.org/licenses/by/4.0/).

Nomenclature

Abbreviations

ASHP	Air-Source Heat Pump
ESC	Extremum-Seeking Control
KPI	Key Performance Indicator
MPC	Model Predictive Control
PI	Proportional-Integral
RMSE	Root Mean Square Error

Greek Letters

ΔL_p	Acoustic discomfort (dB(A)h/d)
Δt_k	Duration of time step (s)
Δ	Time variation (–)
δ	Deviation (–)

Roman Letters

$\dot{Q}$	Heat flow (kW)
d	Distance (m)
e	Control deviation (–)
i	Integral (–)
j	Index of predicted time step (–)
k	Index of time step (–)
K_P	Proportional term (–)
L_p	Sound pressure level (dB(A))
N	Prediction horizon (–)
n	Number (–)
P	Power consumption (kW)
$SCOP$	Seasonal coefficient of performance (–)
T	Temperature (°C)
t_I	Integral term (1/s)
TD	Thermal discomfort (Kh/d)
u	Manipulated value (–)
V	Volume (L)
v	Specific volume (L/kW)

Subscripts

amb	Ambient
BS	Buffer Storage
Comp	Compressor
Cond	Condenser
days	Days
el	Electrical
GB	Grey-Box
int	Internal
LR	Linear regression model
nom	Nominal
opt	Optimal
Pump	Pump
set	Set-Value
sol	Solar
Starts	Compressor starts
std	Standard
top	Upper part
V	Valve
WB	White-Box
w	Weight
Zone	Zone
max	Maximum
min	Minimum

diameters in heat exchangers increase turbulence, thereby amplifying low-frequency and tonal noise. They recommend using smaller tube diameters to mitigate noise, reporting a 2 dB reduction in acoustic emissions when the diameter was decreased from 12 mm to 9.52 mm; however, this reduction must be balanced against potential impacts on thermodynamic efficiency and cost. Gustafsson et al. [16] theoretically studied the effect of heat exchanger design on noise emissions in air-source heat pumps. They found that flat tube heat exchangers are significantly quieter, needing less than half the volume for the same heat capacity compared to common round tube heat exchangers. Additionally, plain fins were shown to be preferable over wavy fins for minimizing noise, though the impact of fin type was relatively small.

Additional research has focused on compressor noise [17–20]. For instance, Park and Wang [17] studied structure-borne noise reduction in rotary compressors through modal analysis and structural optimization. They identified key resonance modes corresponding to peak noise levels and employed topology optimization to avoid these modes by inserting a block-shaped component between the accumulator and compressor. Additionally, optimizing the transfer path between noise emission and immission can be achieved by refining the heat pump housing construction to better insulate and dampen sound. Rahmani et al. [18] investigated the effectiveness of expansion silencers in reducing pulsating noise from reciprocating compressors. They demonstrated that increasing the silencer diameter significantly enhances sound transmission loss, achieving sound dampening at a frequency of 500 Hz from 10 dB (3.7 cm) to 20 dB (7 cm), by reflecting more of the input sound energy. Moreover, the placement of ASHPs plays a significant role in noise reduction, as strategic positioning can minimize the impact of noise on the surrounding environment [6,21].

Further, **control optimization** strategies have been introduced to reduce heat pump noise levels. Manufacturers have developed dedicated control modes (silent mode), which lower fan and compressor speeds to reduce sound emissions [22]. According to Gindre et al. [22], at a stationary operating point of A7W55, silent mode reduces the sound power level of a commercial heat pump by 5 dB(A) while decreasing the heating capacity from 7.3 kW to 5.4 kW. To maintain thermal comfort, this reduction in heating capacity must be compensated by an electrical heater. Consequently, in this case, noise reduction comes at the expense of reduced efficiency or compromised thermal comfort. Silent mode is typically activated based on the time of day, as configured by the installer or user [23,24].

Vering et al. [25] introduce a refrigerant cycle controller which optimizes compressor and evaporator fan speeds to simultaneously enhance energy efficiency and reduce noise emissions while maintaining thermal comfort. The controller builds on the concept that a constant heating capacity can be maintained at varying compressor and fan speeds, each combination affecting energy efficiency and noise levels. By employing an Extremum-Seeking Controller (ESC), they enhance energy efficiency by 3.75% and reduce noise by up to 10.9 dB(A), effectively halving the perceived volume. However, this approach is limited to optimizing the refrigerant cycle controller, leaving the broader potential for system-level flexibility unaddressed.

Recognizing the importance of system-wide control optimization, numerous studies have explored the interaction between heat pump systems and buildings, with a focus on maximizing energy efficiency through the use of flexibility potential [26–30]. A particularly prominent method is Model Predictive Control (MPC) because of its ability

Table 1
Comparison of related works in the literature on control optimization for heat pump systems (non-exhaustive). *Conventional MPC* refers to approaches using physical or semi-physical process models, while *Data-driven MPC* relies on black-box models trained on system data.

Author	System	Algorithm	Target
Mbuwir [34]	Heat pump system	Conventional MPC	Efficiency
Mugnini [27]	Heat pump system	Conventional MPC	Efficiency
Kuboth [28]	Heat pump system	Conventional MPC	Efficiency
Wang [37]	Heat pump system	Conventional MPC	Efficiency
Klepic [38]	Heat pump system	Conventional MPC	Efficiency
Bünning [39]	Heat pump system	Data-Driven MPC	Efficiency
Göbel [36]	Heat pump system	Data-Driven MPC	Efficiency
Prášek [40]	Refrigerant cycle	Conventional MPC	Efficiency
Vering [25]	Refrigerant cycle	Extremum-Seeking Control	Efficiency, Acoustic
This work	Heat pump system	Data-Driven MPC	Efficiency, Acoustic

to consider constraints, prediction of disturbances, and multiple conflicting objectives, such as indoor thermal comfort and building energy demand [31,32]. In MPC, future behavior of a system is predicted with a process model and the control inputs are optimized at each step to minimize a cost function [33]. In a field test study Mbuwir et al. [34] demonstrate MPC's effectiveness in a multi-source heat pump system, leveraging system flexibility introduced by thermal storage tanks and achieve a 7% reduction in electricity consumption compared to a reference controller. The authors employ semi-physical process models and stress that obtaining reliable results demands accurate models, which can make development time-consuming and limit replicability across different settings. By employing data-driven models in the process modeling, the challenges associated with traditional model formulation and calibration can be bypassed [35]. Göbel et al. [36] demonstrate the effectiveness of a data-driven MPC for heat pump systems within hardware-in-the-loop experiments. In an initial system identification process, the authors utilize a reference controller to generate six weeks of simulated training data, which is then used to train data-driven process models (artificial neural networks). Their MPC approach directly controls compressor speed to maintain a room temperature between comfort bounds. The controller improves energy efficiency by up to 20.25% over a traditional control concept with a heating curve. The improved efficiency stems from the controller's ability to integrate internal gains and solar radiation into its operational strategy.

While literature shows that MPC is a promising method, most existing applications focus primarily on optimizing energy efficiency (see Table 1), with limited attention given to heat pump acoustics. To address this gap, the present study introduces an MPC approach that optimizes the interaction between a heat pump system and a building, considering both energy efficiency and noise emissions. Therefore, this work contributes to improving the heat pump system controller as follows:

- We introduce a novel implementation of a heat pump system controller based on data-driven MPC. This controller optimizes both heat pump acoustics and energy efficiency of an ASHP while maintaining thermal comfort by leveraging system flexibility.
- We explore various cost function formulations and compare two MPC formulations with a reference controller, quantifying improvements in energy efficiency, acoustic emissions, and thermal comfort.
- We verify the performance of the model predictive controller through a simulation study that evaluates two different heat pump placement configurations, assessing its transferability to diverse scenarios.

The paper is structured as follows: Section 2 presents the simulation model. Section 3 details the problem formulation of the MPC, including the design of the cost function and process model training. Section 4 introduces the case study design. Section 5 presents the results. Section 6 discusses the investigated controllers and lists current limitations. Finally, Section 7 summarizes the findings.

2. Modeling of the building energy system

In this section, we present the modeling approach for the building energy system. The models are developed using the object-oriented programming language Modelica, implemented within the Dymola software. The simulation utilizes the Building Energy System Modules (*BESMod*) [41] library, which enables the integration of various open-source libraries for physical modeling in Modelica. For this study, models from the *BuildingSystems* [42], *Buildings* [43], *IDEAS* [44], *IBPSA* [45], *TEASER* [46], and *AixLib* [47] libraries are integrated and employed within *BESMod*. A comprehensive table listing model names, relevant parameters, and the source library is given in Table A.6 and the version of the used Modelica Libraries is indicated in Table A.7.

Fig. 1 illustrates the schematic structure of the building's energy system consisting of a heat pump, a buffer storage, a heat transfer system (underfloor heating) and a building. Pumps operate at fixed speed to circulate water between the subsystems. The water flow rate passing the underfloor heating can be controlled with a valve. Additionally, the compressor speed of the heat pump can be adjusted, which affects both heating capacity and sound emissions. In the following, a brief description of the models is presented.

Heat Pump Model:

The heat pump is modeled both thermodynamically and acoustically. The thermodynamic modeling employs a characteristic map approach (Wüllhorst et al. [48]) which calculates heating capacity and power consumption based on ambient temperature, supply temperature, and compressor speed. The characteristic map (see Tables A.8 to A.13) is based on measurement data of a commercially available monoblock ASHP with nominal heating capacity of 11.2 kW. The device was measured on a hardware-in-the-loop test bench under 15 stationary conditions. Information about the test bench setup can be derived from Vering et al. [49]. Further, the thermal inertia of heat exchangers and compressor is modeled with first-order filter. Frost formation is not considered for simplicity.

Additionally, the heat pump model outputs sound emissions as a function of power consumption. Therefore, acoustic measurements were performed using four microphones, placed equidistantly at a distance of one meter around the heat pump. To account for the disruptive influence of reflective walls of the test chamber, reference measurements were taken using a sound source with known sound power, and the influence was corrected. Based on the sound pressure levels recorded by the microphones from compressor and fan, the A-weighted sound power level of the heat pump was determined in accordance with DIN EN ISO 3743 [50]. Fig. 2 depicts the sound power level as a function of power consumption of the heat pump. The relationship between sound power level and power consumption is incorporated into the simulation model using a polynomial function. The sound source cannot be distinguished as originating from the compressor or the fan, thus only the compressor speed is controlled.

Buffer Storage Model:

A buffer storage tank is implemented to temporally decouple heat demand from generation. The stratified tank is modeled using a finite

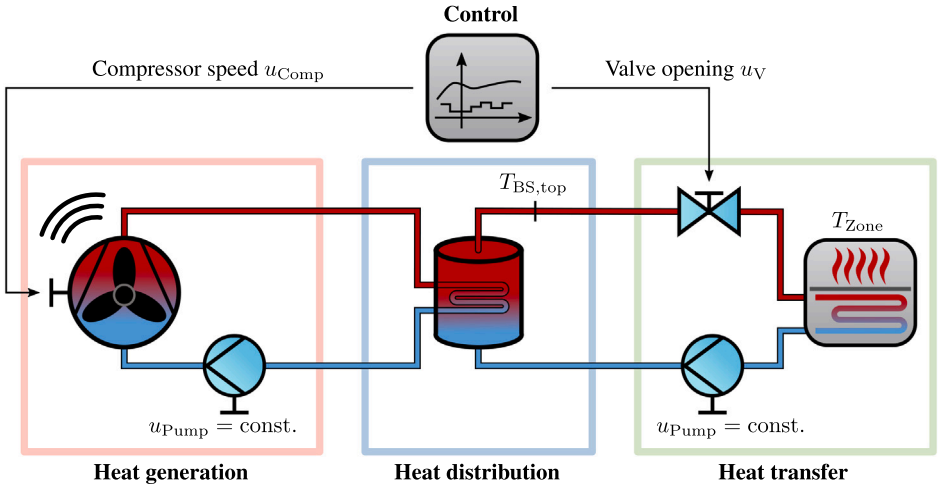


Fig. 1. Schematic structure of the building energy system. The compressor speed and the valve opening in the secondary heating circuit are controlled by the system controller.

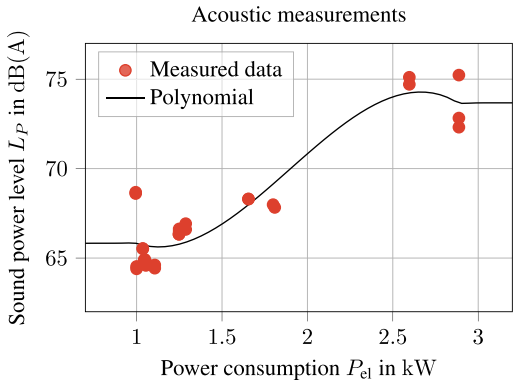


Fig. 2. Sound power level as a function of the heat pump's power consumption, based on acoustic measurements conducted in a test lab. This correlation is integrated into the simulation model to simulate the acoustic behavior of the heat pump.

volume approach and incorporating a buoyancy model to account for heat transfer between discretized layers. Additionally, thermal losses to the surroundings are represented. The heat pump charges the storage tank through a coiled tube heat exchanger located within the tank. The storage has a specific volume of 70 l/kW, exceeding the typical range of 12 to 35 l/kW as per DIN EN 15450 [51]. This larger size aims to enhance load shifting potential. Government incentives like the German Federal Government offer bonuses for systems with storage capacities of 30 l/kW and above, promoting larger buffer storages [52].

Building Model:

The building model determines a heat demand based on outdoor temperature, solar radiation, and internal gains. The building is represented as a reduced-order model and is generated with the open-source tool *TEASER* [46] which is based on the method developed by Loga et al. [53]. The building's heat demand is simulated using weather data from a reference year for Potsdam, Germany [54].

Underfloor Heating Model:

The underfloor heating system is modeled using a finite volume approach, where the pipe is discretized into a series of elements. Heat transfer occurs via convection, conduction, and radiation between the pipe elements and the room, with additional heat conduction to the ground, which is assumed to have a constant temperature. Each element includes thermal capacities for both the room and the ground.

3. Data-driven model predictive control for heat pump systems

We apply the Python-based framework developed by Stoffel et al. [55]. Within the framework Modelica models are integrated as black-box Functional Mockup Units (FMUs) [56]. The MPC employs separate process models to predict system states, forming the basis for calculating the optimal control trajectory, which is then fed to the FMU. Section 3.1 introduces the optimal control problem and defines a modular cost function. Section 3.2 outlines the process of developing the process models.

3.1. Formulation of the optimal control problem

Fig. 3 illustrates the data processing flow chart of the MPC. The MPC calculates control trajectories for compressor speed and valve opening based on ambient temperature T_{amb}, internal heat gains $\dot{Q}_{\text{int}}$, and solar radiation heat gains $\dot{Q}_{\text{sol}}$. Further, the actual buffer storage temperature ($T_{\text{BS,top}}$) and zone temperature (T_{Zone}) from the previous time step serve as an input. Four process models convert these inputs into process variables, which are then used by the optimizer to calculate the optimal control values the compressor speed u_{Comp} and valve opening u_{V}.

Eqs. (1a) to (1e) show the functional relationships for each process model as shown in Fig. 3. For clarity, the following equations are given for a single prediction step j without time lagged values. The process model output is displayed by $f(\cdot)$. The prediction horizon N is set to one day. With a sampling rate of ten minutes, this corresponds to $N = 144$.

$$T_{\text{Zone},j+1} = T_{\text{Zone},j} + f(u_{\text{V},j}, T_{\text{Zone},j}, T_{\text{BS,top},j}, T_{\text{amb},j}, \dot{Q}_{\text{int},j}, \dot{Q}_{\text{sol},j}) \tag{1a}$$

$$T_{\text{BS,top},j+1} = T_{\text{BS,top},j} + f(u_{\text{V},j}, u_{\text{Comp},j}, T_{\text{Zone},j}, T_{\text{BS,top},j}) \tag{1b}$$

$$P_{\text{el},j+1} = f(u_{\text{Comp},j}, T_{\text{BS,top},j}, T_{\text{amb},j}) \tag{1c}$$

$$L_{p,j+1} = f(P_{\text{el},j}) \tag{1d}$$

$$\forall\, j \in [0,\, N-1] \tag{1e}$$

The optimization of compressor speed and valve opening is performed based on the cost function, which is formulated in Eq. (2).

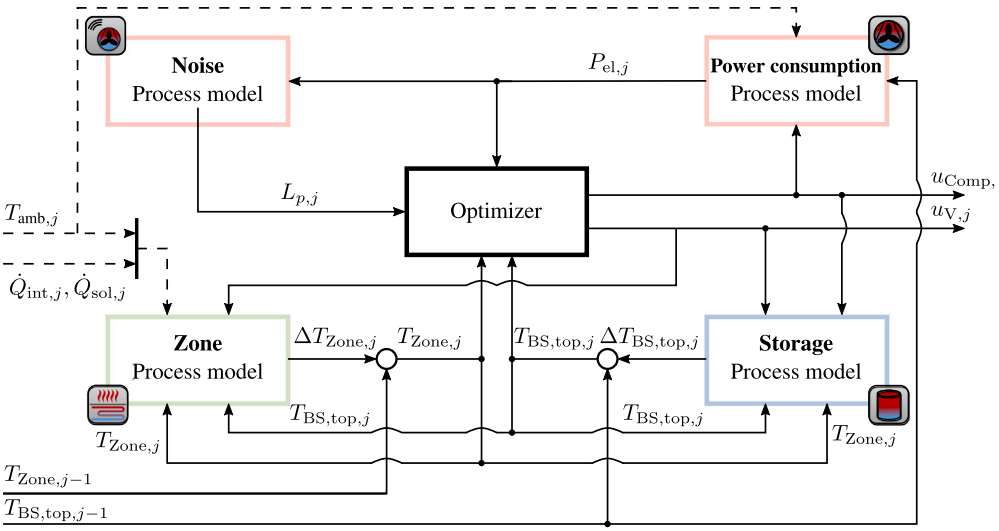


Fig. 3. Scheme of the model predictive controller for one time step. The colors of the process models correspond to Fig. 1. Measured values are marked as dashed lines.

$$
\begin{aligned}
(u_{\mathrm{Comp}}, u_{\mathrm{V}})_{\mathrm{opt}} = \arg\min_{u_{\mathrm{Comp}}, u_{\mathrm{V}}} \sum_{j=0}^{N} & \underbrace{w_{T_{\mathrm{Zone}}} \cdot \delta^2_{T_{\mathrm{Zone}},j}}_{\text{Thermal Discomfort}} + \underbrace{w_{P_{\mathrm{el}}} \cdot \frac{P_{\mathrm{el}}}{P_{\mathrm{el,max}}}}_{\text{Electric Power}} \\
& + \underbrace{w_{T_{\mathrm{BS,top}}} \cdot \frac{T_{\mathrm{BS,top},j} - T_{\mathrm{BS,top,min}}}{T_{\mathrm{BS,top,max}} - T_{\mathrm{BS,top,min}}}}_{\text{Buffer Storage toptemperature}} \\
& + \underbrace{w_{L_p} \cdot \delta^2_{L_p,j}}_{\text{Acoustic Discomfort}} + \underbrace{w_{u_{\mathrm{Comp}}} \cdot \delta^2_{u_{\mathrm{Comp}}}}_{\text{Compressor speed}} + \underbrace{w_{u_{\mathrm{V}}} \cdot u_{\mathrm{V}}}_{\text{Valve-position}}
\end{aligned} \tag{2}
$$

For each time step k, the cost function is optimized over each prediction step j up to the prediction horizon N. The optimizer calculates the optimal control variables (compressor speed u_{Comp} and valve opening u_{V}) for each predicted step j, and the calculated control variables at time step k are applied to the system. The modular cost function can be adapted based on the application needs, with terms that can be prioritized or deactivated through weights w_i. Except for the first summand, we normalize all cost function variables to values between zero and one. Table A.15 shows the parameters of the cost function.

To minimize thermal discomfort, deviations in zone temperature T_{Zone} are penalized. For energy-efficient operation, power consumption P_{el} and buffer storage temperature $T_{\mathrm{BS,top}}$ are included in the cost function. To ensure quiet operation, high sound pressure limits exceeding legal limits and compressor speeds above a defined threshold $\delta_{u_{\mathrm{Comp}}}$ may be considered in the cost function. Additionally, penalizing the valve opening u_{V} helps effectively load the storage and, therefore, limit noise levels for a certain amount of time.

Instantaneous thermal discomfort $\delta_{T_{\mathrm{Zone}}}$ and acoustic discomfort δ_{L_p} are deviations from the thermal and acoustic comfort bounds. Eqs. (3a) to (3e) describe $\delta_{T_{\mathrm{Zone}}}$, δ_{L_p} and $\delta_{u_{\mathrm{Comp}},j}$. We penalize those terms quadratically to avoid large deviations.

$$T_{\mathrm{Zone,min},j} - \delta_{T_{\mathrm{Zone}},j} \leq T_{\mathrm{Zone},j} \leq T_{\mathrm{Zone,max},j} + \delta_{T_{\mathrm{Zone}},j} \tag{3a}$$

$$\frac{L_{p,\mathrm{min},j}}{L_{p,\mathrm{max,WP}}} - \delta_{L_p,j} \leq \frac{L_{p,j}}{L_{p,\mathrm{max,WP}}} \leq \frac{L_{p,\mathrm{max},j}}{L_{p,\mathrm{max,WP}}} + \delta_{L_p,j} \tag{3b}$$

$$\delta_{u_{\mathrm{Comp}},j} = \max(u_{\mathrm{Comp,max},j} - u_{\mathrm{Comp},j}, 0) \tag{3c}$$

$$0 \leq \delta_{T_{\mathrm{Zone}},j}, \delta_{L_p,j} \tag{3d}$$

$$\forall\, j \in [0,\, N] \tag{3e}$$

Additionally, the optimal control problem includes fixed constraints (Eqs. (4a) to (4d)). These constraints cover the maximum and minimum values of the control variables. The relative compressor speed u_{Comp} ranges from 0 ($u_{\mathrm{Comp,min}}$) to 1 ($u_{\mathrm{Comp,max}}$). If u_{Comp} falls below a threshold $u_{\mathrm{Comp,off}} = 0.334$, the heat pump is switched off. This results in cycling behavior during low load conditions. Further, the storage head temperature is constrained to ensure operation within the compressor envelope.

$$u_{\mathrm{V,min},j} \leq u_{\mathrm{V},j} \leq u_{\mathrm{V,max},j} \tag{4a}$$

$$u_{\mathrm{Comp,min},j} \leq u_{\mathrm{Comp},j} \leq u_{\mathrm{Comp,max},j} \tag{4b}$$

$$T_{\mathrm{BS,top,min},j} \leq T_{\mathrm{BS,top},j} \leq T_{\mathrm{BS,top,max},j} \tag{4c}$$

$$\forall\, j \in [0,\, N-1] \tag{4d}$$

The weights of the terms of the cost function are determined with a sensitivity analysis described in Section 4.1.

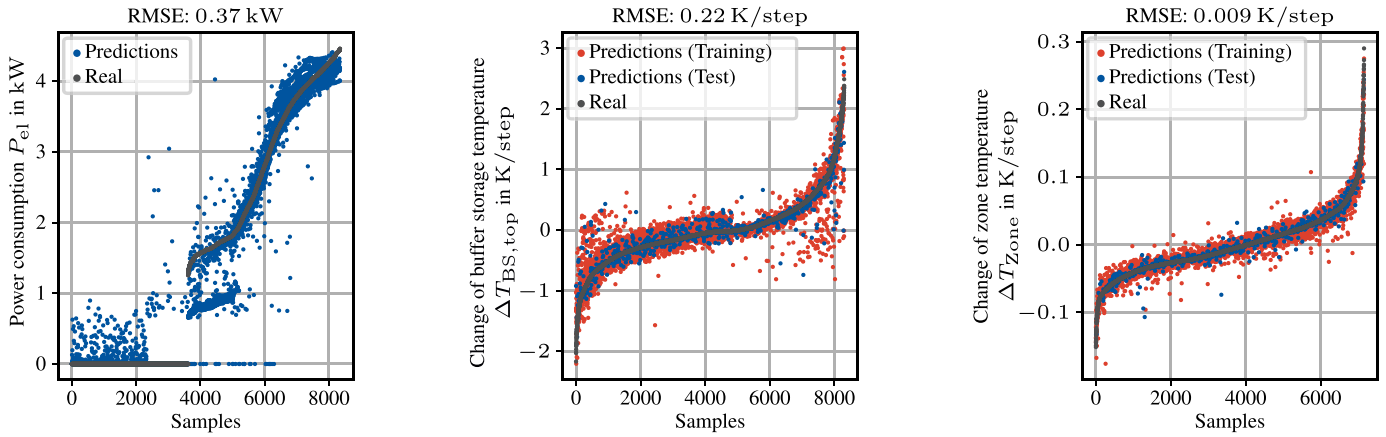
3.2. Training of data-driven process models

Accurate process models are essential for aligning the optimizer's control trajectory with the optimal control strategy of the real system (as described in Section 2). However, developing these models involves a trade-off between modeling effort and accuracy. In this work, data-driven methods are utilized to minimize the complexity of model creation while maintaining adequate accuracy. Training data is generated in advance using a reference controller, and this data is used to develop the process models. Details on the data generation procedure are provided in Appendix B. We test various model types including linear regression, Gaussian process regression (GPR), artificial neural networks (ANN), and simplified grey-box models. Recognizing computational constraints (as further discussed later), we explored several configurations for the artificial neural networks and Gaussian process regressions, selecting models based on their performance. Table 2 lists the RMSE values for all investigated model types for each process model. Appendix C depicts training results for all investigated model types for each process model.

The final process models were selected based on model accuracy, computational complexity, and robustness. While GPR and ANN demonstrated high accuracy during testing, they exhibited limitations in robustness which describes the stability and reliability of model performance across the full range of operating conditions over an entire heating season. Both GPR and ANN models produced implausible outputs when extrapolating beyond the training data, resulting

Table 2
Process model accuracy depending on model type.

Process model	RMSE			
	Linear regression	Gaussian process regression	Neural Network	Grey-Box
Electrical power	0.44 kW	0.19 kW	0.25 kW	0.37 kW
Storage temperature	0.22 K/step	0.42 K/step	0.12 K/step	–
Zone temperature	0.009 K/step	0.016 K/step	0.01 K/step	–



(a) Electrical Power (Grey-Box). (b) Storage temperature (Linear Regression). (c) Zone temperature (Linear Regression).

Fig. 4. Training results for the final process models. The blue and red dots represent the predicted values of each model during the test and training phase. Since the electrical power model is not data-driven no training phase is required. The grey dots represent the real values meaning a high accuracy of process models results in small differences to the colored dots.

in unstable controller behavior. To ensure consistent and physically meaningful results, we selected linear regression models for the storage temperature and zone temperature process models, as they exhibited robust behavior across all relevant operating conditions. Additionally, these models significantly reduced computational complexity, thus increasing simulation speed.

For the power consumption process model, we selected a grey-box approach based on compressor speed and temperature lift (i.e., the temperature difference between the storage and the environment), both multiplied by fitting factors. The temperature lift reflects the influence of the pressure ratio (inlet and outlet pressure) on compressor power. If the relative compressor speed u_{Comp} falls below the turn-off speed $u_{\mathrm{Comp,off}}$, the heat pump is switched off, and no electrical power is consumed. This on–off behavior is captured by the exponential term in the equation, which smoothly transitions the power consumption to zero as the compressor speed approaches the shutoff threshold:

$$P_{\mathrm{el}} = \left(3400 \cdot u_{\mathrm{Comp}} + 0.4 \cdot (T_{\mathrm{BS,top}} - T_{\mathrm{amb}})^2\right) \cdot \frac{1}{1 + \exp\left((u_{\mathrm{Comp,off}} - u_{\mathrm{Comp}}) \cdot 100\right)} \tag{5}$$

The acoustic process model is identical to the correlation implemented in the simulation model (see Section 2). 4 shows the training results of all final process models.

4. Case study

We investigate two distinct MPC formulations across two heat pump placement scenarios. In addition, we evaluate a state-of-the-art reference controller. Each simulation spans an entire heating period typical for Germany (7 months, October to April).

4.1. Placement scenarios

To evaluate the MPC's ability to adapt to changing conditions, we examine two heat pump placement scenarios relative to the building. Specifically, we vary the distance between the noise emission (heat pump) and the noise immission (building). This variation affects the sound pressure level at immission as depicted in Fig. 5. Sound pressure levels are calculated based [57,58] from sound power level (see Fig. 2). Additionally, the figure includes noise limits specified by German regulations for residential areas, allowing up to 50 dB(A) during the day (6 a.m. to 10 p.m.) and 35 dB(A) at night (10 p.m. to 6 a.m.) [59]. The noise limits are considered in Eq. (3b) as upper limits for the sound pressure level $L_{p,\max,j}$ depending on the time of the day. These placement scenarios necessitate different MPC operational strategies to ensure compliance with noise regulations.

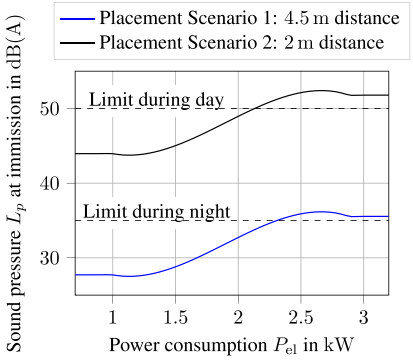
4.2. Data reduction

In the context of this work, the evaluation variables are either specified as average values or are divided by the number of simulated days n_{days}. The duration of an interval k is denoted by Δt_k. As time series with discrete-time values are generated and analyzed in this work, the KPIs are displayed in the form of sums instead of integrals. The $SCOP$ describes the average efficiency of the heat pump depending on the heating capacity $\dot{Q}_{\mathrm{Cond},k}$ and the power consumption $P_{\mathrm{el},k}$. The following calculation rule is used.

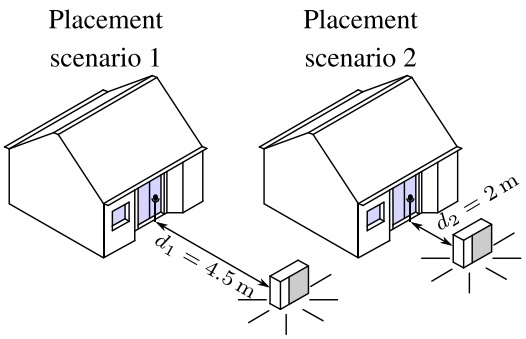
$$SCOP = \frac{\sum_{k=1}^{n} \Delta t_k \cdot \dot{Q}_{\mathrm{Cond},k}}{n_{\mathrm{days}} \cdot \sum_{k=1}^{n} \Delta t_k \cdot P_{\mathrm{el},k}} \qquad [SCOP] = - \tag{6}$$

The cumulative thermal discomfort TD describes the deviation of the zone temperature from the tolerated temperature band. The system can be actively overloaded to shift noise emissions over time. For this reason, deviations upwards and downwards are understood as discomfort. The average thermal discomfort per day can be calculated using the following equation.

$$TD = \frac{1}{n_{\mathrm{days}}} \cdot \sum_{k=1}^{n} \Delta t_k \cdot \delta_{T_{\mathrm{Zone},k}}, \qquad [TD] = \mathrm{Kh/d} \tag{7}$$



(a) Sound pressure level for both placement scenarios based on the power consumption.



(b) Distance from heat pump to house for both analyzed use cases [60].

Fig. 5. Noise immission at the building for two heat pump placement scenarios, illustrated by distance between heat pump and place of immission [60]. For distal installation (4.5 m), regulatory limits are exceeded at night under high power consumption. For proximal installation (2 m), nighttime operation and daytime operation at high power consumption exceeds limits. Both polynomials are extrapolated at constant values when the power consumption is outside of measured values.

In addition, the acoustics of the systems are to be evaluated. For this purpose, the cumulative acoustic discomfort is used based on the thermal discomfort. The acoustic discomfort is calculated according to the following equation from the time-dependent upper limit $L_{p,\max,k}$ from the German administrative regulation "TA Lärm" [59] and the actual sound pressure level $L_{p,k}$.

$$\Delta L_p = \frac{1}{n_{\text{days}}} \cdot \sum_{k=1}^{n} \Delta t_k \cdot \max(0, L_{p,k} - L_{p,\max,k}) \qquad [\Delta L_p] = \text{dB(A)h/d} \qquad (8)$$

The number of average compressor starts per day n_{starts} is also considered, as frequent starts can reduce the service life of the compressor [61]. Compressor starts are excluded from penalties in the cost function, but should nevertheless be analyzed in order to identify possible disadvantages of control concepts.

4.3. Controller design

Two MPCs, as described in Section 3, and a reference controller are evaluated. The MPCs differ in the weighting factors w used in the cost function (see Eq. (2)). The following section outlines the controllers, followed by a description of the procedure used to determine the weighting factors.

- **MPC-Efficiency**: The first MPC aims to provide heat efficiently while maintaining thermal comfort. This involves penalizing thermal discomfort, the electrical energy consumption of the heat pump, and the storage tank's head temperature. The comfort band for the zone temperature T_{Zone} is defined with a minimum of $T_{\text{Zone,min}} = 20\,°\text{C}$ and a maximum of $T_{\text{Zone,max}} = 22\,°\text{C}$. Above the value thermal discomfort as defined in Eq. (3a) occurs.
- **MPC-Acoustic**: The second MPC, prioritizes a reduction in acoustic discomfort over efficiency while maintaining thermal comfort. The thermal comfort is defined as for MPC-Efficiency. The acoustic discomfort results from the difference between the actual immission and the time-dependent permitted limit values according to Fig. 5.
- **Reference controller**: A typical controller consisting of hysteresis, heating curve, and PI controller is designed. A schematic representation is illustrated in Fig. A.15. The storage head temperature is controlled by the compressor speed using a PI controller and a hysteresis with a bandwidth of 5 K. The set temperature of the storage head temperature is derived from a heating curve. The heating curve is based on the building's nominal supply temperature and ensures operation without thermal comfort losses. A continuous PI controller is used to set the valve opening according to the zone temperature. The reference controller maintained a constant zone temperature setpoint of 20 °C. This value served as a standardized baseline for comparative analysis, as both MPCs were designed to reduce zone temperature. The reference controller operated without accounting for acoustic emissions, reflecting common practices in current building management systems. Furthermore, the PI controller parameters were manually tuned to optimize performance, achieving a balance between responsiveness and stability by minimizing oscillations and maintaining rapid reaction times (values are given in Table A.14).

In order to determine the cost function weights w that achieve the desired behavior of the MPCs, we performed a sensitivity analysis. The weight for zone temperature $w_{T_{\text{Zone}}}$ is set to one as a reference point. The procedure for the sensitivity analysis is as follows:

1. Select potential values for each weight w (see Table D.16).
2. Evaluate all possible combinations (full factorial design) over a five-day representative period (refer to Fig. D.20).
3. Select the final set of weights for the MPC using relevant KPIs specified in Section 4.2.

In the following paragraphs, we discuss the final selection of the weights for the Acoustic-MPC at proximal installation. Fig. 6 shows the $SCOP$, the thermal discomfort TD and the acoustic discomfort ΔL_p at proximal installation for a variation of the acoustic discomfort penalty (w_{L_p}). Low values for w_{L_p} (<3) lead to high acoustic discomfort and high $SCOP$. Contrary higher values for w_{L_p} (>3) lead to a reduction in acoustic discomfort but also a reduction in $SCOP$. Hence, a conflict of objectives between low acoustic discomfort and high efficiency exists. For very high w_{L_p} values (>30), acoustic discomfort increases again, indicating that excessively steep optimization gradients can prevent convergence to an optimal solution. Based on this analysis, we select $w_{L_p} = 10$, as it achieves the lowest acoustic discomfort while preserving a reasonable $SCOP$ and thermal discomfort.

Fig. 7 shows the relevant KPIs for different values of the weight the power consumption $w_{P_{\text{el}}}$. A decrease of the weight leads to higher $SCOP$ values and higher thermal discomfort throughout the testing period which is we expected. In comparison to the acoustic discomfort weight w_{L_p}, the weight of the power consumption $w_{P_{\text{el}}}$ seems to have a greater sensitivity on thermal discomfort, since at lower numerical values, the thermal discomfort is more than four times higher compared to Fig. 7. A conflict of objectives similar to Fig. 6 is displayed for high weights ($>10^{-1}$). Interestingly, at lower values increasing the power

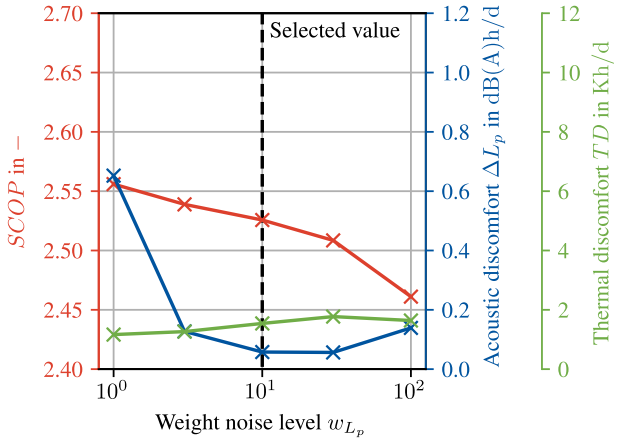


Fig. 6. KPIs of Acoustic MPC (placement scenario 1: proximal installation) in relation to the weight of the noise level during the analyzed five days. The selected value is marked by a vertical dashed line.

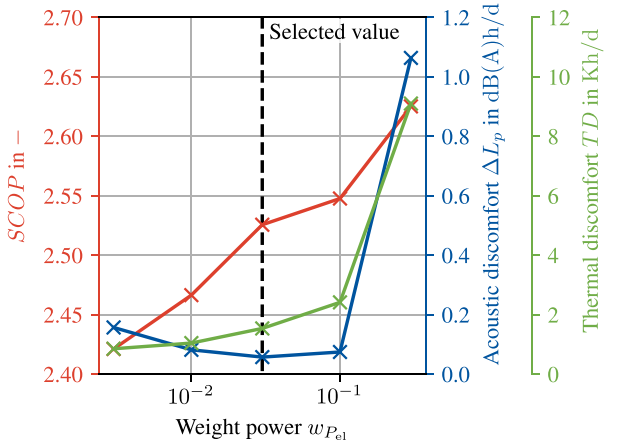


Fig. 7. KPIs of Acoustic MPC (placement scenario 1: proximal installation) in relation to the weight of the power consumption during the analyzed period. The selected value ($w_{P_{el}} = 0.03$) is marked by a vertical dashed line.

consumption weight $w_{P_{el}}$ reduces the acoustic discomfort. Therefore, we select $w_{P_{el}} = 10^{-2}$.

Fig. 8 shows the impact of changing the weight of the valve opening w_{u_V}. Since the weights are evaluated at all possible combinations we selected only three values. A value of $w_{u_V} = 10^{-3}$ is selected since it results in low acoustic discomfort and a high $SCOP$ value while maintaining reasonable thermal discomfort.

Steps 1–3 were carried out for both MPCs. Additionally, for the Acoustic-MPC, the analysis was performed for both placement scenarios to assess the robustness of the weighting factors under different optimization conditions. The final weights are presented in Table 3.

5. Simulation results

In the following section, we present and analyze the simulation results. The focus initially lies on Case Study I, which examines the distal installation of the heat pump (placement scenario 1). Case Study II evaluates the impact of installing the heat pump closer to the building (placement scenario 2), resulting in higher sound pressure levels.

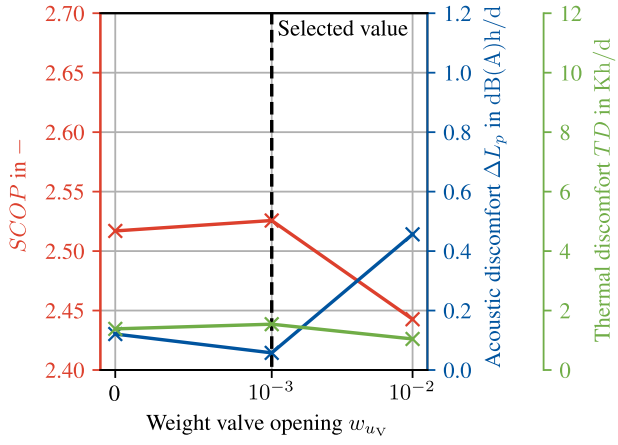


Fig. 8. KPIs of Acoustic MPC (placement scenario 1: proximal installation) in relation to the weight of the valve opening during the analyzed period. The selected value ($w_{u_V} = 10^{-3}$) is marked by a vertical dashed line.

5.1. Case study I: Distal installation

We compare the reference controller, the Efficiency-MPC and the Acoustic-MPC at placement scenario 1. Fig. 9 shows the zone temperature T_{Zone} and the storage temperature $T_{\text{BS,top}}$ for two characteristic days in January, during which the ambient temperature T_{amb} fluctuated between −0.3 °C and 7 °C.

Reference Controller: From 9 a.m. to 12 p.m., the zone temperature deviates upwards due to increased ambient temperature and radiation. From 1 p.m. on, radiation and ambient temperature decrease, resulting in an increasing heating demand. Since the reference controller cannot see the future, the valve can only be closed as soon as the zone temperature T_{Zone} falls below 20 °C, leading to thermal discomfort. The heat pump begins to cycle at around 1 p.m. due to lower heating demand, resulting in the displayed non-steady course of the buffer storage temperature.

Efficiency-MPC: The zone temperature is maintained at approximately 20 °C. The MPC aims to lower storage temperatures since low temperature lifts result in higher efficiency. In comparison to the reference controller, the buffer storage temperature is on average reduced by 7 K. Since the controller predicts the system behavior, we observe storage temperatures of below 30 °C during 11 a.m. and 4 p.m. because of radiation and increasing ambient temperatures.

Acoustic-MPC: The storage temperatures are similar to those recorded under Efficiency-MPC for most parts of the day. Around 7 p.m., the controller increases storage temperatures to use the generated heat during nighttime while minimizing noise levels. For the displayed days, the storage temperature reaches a maximum value of 46 °C and 44 °C. From approximately 10 p.m. to 12 a.m., the storage temperature decreases strongly because the heat pump is switched off. From 12 a.m. on, the storage temperature is maintained at around 35 °C, which results in thermal discomfort.

We compare the controller over the whole heating period using heatmaps. Fig. 10 illustrates the buffer storage temperature, with subfigures for Efficiency-MPC and Acoustic-MPC.

We observe higher buffer storage temperatures during December and January due to colder temperatures compared to other months with every controller. The yearly course of solar radiation is visible in the Efficiency-MPC scenario (Fig. 10(a)), as buffer storage temperatures decrease during the day, especially in October and April. The temperature remains below 41 °C throughout the whole heating period resulting in low temperature lifts and therefore high energy efficiency of the heat pump.

Table 3
Final weighting factors determined from sensitivity analysis. In general, thermal and acoustic discomfort are penalized higher than power consumption and valve opening for Acoustic-MPC.

Penalty	Weight	Efficiency-MPC Placement Scenario 1/2	Acoustic-MPC Placement Scenario 1	Acoustic-MPC Placement Scenario 2
Thermal discomfort	$w_{T_{\text{Zone}}}$	1	1	1
Acoustic discomfort	w_{L_p}	0	10	1
Power consumption	$w_{P_{\text{el}}}$	0.1	0.03	0.03
Valve Opening	$w_{u_{\text{v}}}$	0	0.001	0.01
Buffer Storage Temp.	$w_{T_{\text{BS,top}}}$	0.03	0	0
Compressor speed	$w_{u_{\text{Comp}}}$	0	10	0

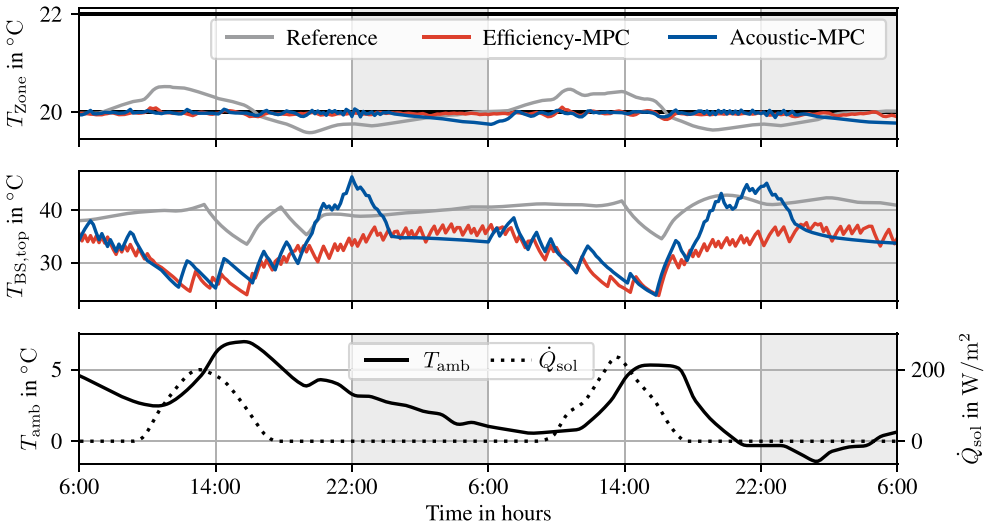
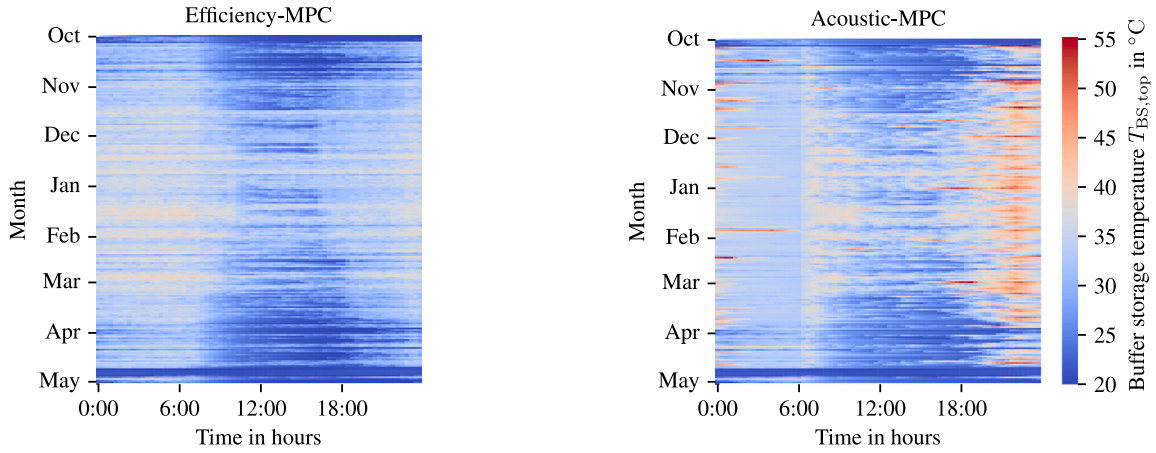


Fig. 9. Comparison of zone temperature T_{Zone} and temperature of the buffer storage $T_{\text{BS,top}}$ for two characteristic days in January. Ambient temperature and solar radiation are displayed to present the impact of the environment on the control systems.



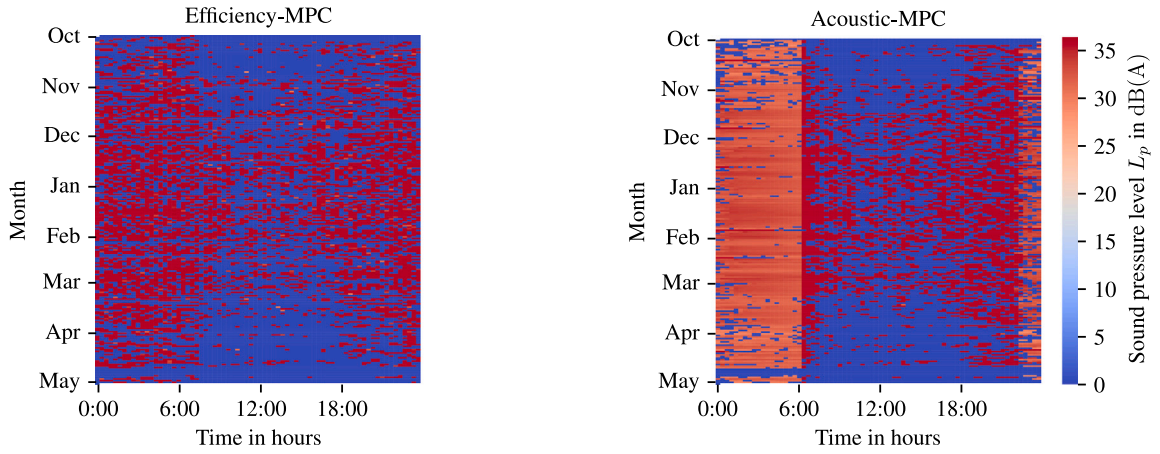
(a) Buffer storage temperature throughout the whole year when applying the Efficiency-MPC.

(b) Buffer storage temperature throughout the whole year when applying the Acoustic-MPC.To reduce noise emissions during the night, the storage is heated in the evening.

Fig. 10. Comparison of the buffer storage temperature of the Efficiency-MPC and the Acoustic-MPC. Both controllers decrease the temperature during the day compared to the reference controller. Due to the sound limits during the night, Acoustic-MPC heats the storage towards the evening.

For Acoustic-MPC (Fig. 10(b)), we can discern the borders of noise levels at 6 a.m. and 10 p.m.. Buffer storage temperature increases until 10 p.m. (with the highest daily temperature recorded at an average of 39 °C). The temperature decreases throughout the night on average by around 6 K. A noticeable increase in temperature occurs after 6 a.m. when the compressor can operate at full load without exceeding allowed noise levels. During daylight hours, buffer storage temperatures remain similar to those observed with Efficiency-MPC.

During the first days of October and late April, the required zone temperatures are achieved through internal and solar radiation gains,



(a) Noise level of the heat pump of the Efficiency-MPC.

(b) Noise level of the heat pump of the Acoustic-MPC.

Fig. 11. Comparison of the immitted noise level at distal installation of the Efficiency-MPC and the Acoustic-MPC. When penalizing the noise level, the compressor is mainly operated in part mode due to lower tolerated sound pressure levels during the night.

eliminating the need for heating due to sufficiently high ambient temperatures; consequently, the heat pump remains switched off.

In Fig. 11 the heatmaps of the sound pressure level are shown, focusing on both Efficiency-MPC and Acoustic-MPC scenarios.

The Efficiency-MPC operates the heat pump mainly during the night, resulting in high sound pressure levels (Fig. 11(a)). Solar radiation is visible during the day, similar to what we observe with storage temperature. The heat pump operates mainly at full load, leading to high sound pressure levels.

When controlled by Acoustic-MPC, part load occurs during the night (Fig. 11(b)), which means the sound pressure level is generally maintained within the limit of 35 dB(A). Towards 6 a.m., the compressor typically operates at constant speeds, resulting in stable sound pressure levels. Higher sound pressure levels are observed after 6 a.m. when heating up both buffer storage and zone and before 10 p.m. to load the storage before restrictions on sound pressure levels take effect.

Fig. 12 illustrates the relationship between $SCOP$, acoustic discomfort, and thermal discomfort (represented by the size of the dots) for the entire year. The total values are summarized in Table 4 for each controller.

For the reference controller, the $SCOP$ is 2.52. Acoustic discomfort registers at 2.08 dB(A)h/d, while thermal discomfort is reported at 2.28 Kh/d. Notably, compressor starts occur over the heating period on average only 2.1 times per day.

Both MPCs show an increase in $SCOP$: Efficiency-MPC demonstrates a 10% increase due to low storage temperatures, while Acoustic-MPC shows a 6% increase. Additionally, both approaches decrease thermal discomfort, with Efficiency-MPC achieving more significant reductions.

In terms of acoustic discomfort, applying Acoustic-MPC results in a decrease of 92%, whereas Efficiency-MPC slightly increases this metric. By applying different weights to the cost function than those in Table 3, we expect a visible Pareto front of the final KPIs in Fig. 12. As previously noted, Efficiency-MPC leads to a high number of compressor starts compared to Acoustic-MPC, which reduces these starts to one-third of those seen with Efficiency-MPC.

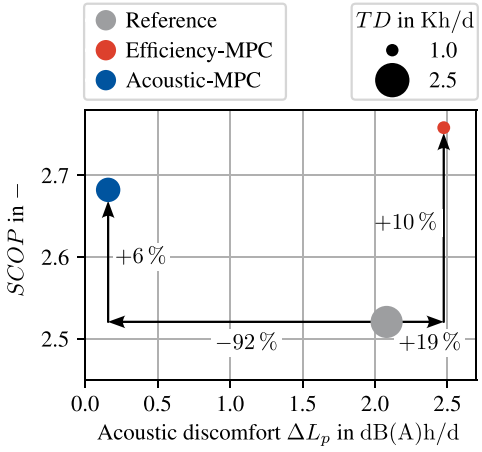


Fig. 12. Comparison of the $SCOP$, acoustic discomfort ΔL_p and thermal discomfort TD (given by the size of the dots) for placement scenario 1. Applying the Efficiency-MPC, the $SCOP$ increases by 0.25 points while the thermal discomfort decreases by 55%. The Acoustic-MPC reaches an improvement of $SCOP$ of 0.16 points and acoustic discomfort of 92% while maintaining similar comfort compared to the reference controller.

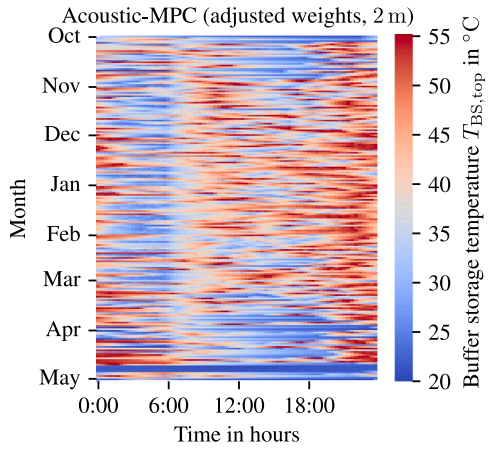
Table 4
KPIs of the simulations for placement scenario 1 (distance between heat pump and home corresponds to 2 m).

KPI & Unit	Reference	Efficiency-MPC	Acoustic-MPC
$SCOP$ in –	2.52	**2.76**	2.68
Acoustic discomfort ΔL_p in dB(A)h/d	2.08	2.47	**0.16**
Thermal discomfort TD in Kh/d	2.28	**1.01**	1.63
Average compressor starts n_{Starts} in 1/d	**2.1**	36.9	12.3
Average buffer storage temperature in °C	38.7	**30.6**	32.4

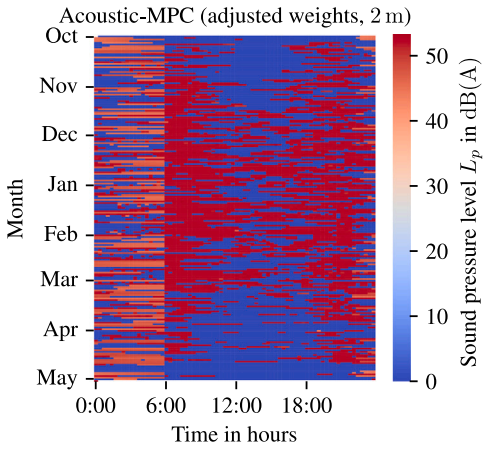
5.2. Case study II: Proximal installation

In this case study, we analyze the installation of the heat pump 2 m away from the house (placement scenario 2), which leads to acoustic discomfort even at part load during the night, which requires that the heat pump be turned off to avoid this discomfort (see Fig. 5). Therefore, we adapted the weights of Acoustic-MPC for a closer installation. We compare the results of the adjusted Acoustic-MPC with the original configuration to evaluate the applicability to new placement scenarios.

Fig. 13 illustrates buffer storage temperature and sound pressure level of the adjusted Acoustic-MPC. The buffer storage temperature



(a) Buffer storage temperature throughout the whole heating period for placement scenario 2.



(b) Sound pressure level (due to the distal installation, the sound pressure level at imission is higher compared to placement scenario 1).

Fig. 13. Buffer storage temperature and sound pressure level resulting from the weight adjustment at proximal installation of the heat pump (placement scenario 2).

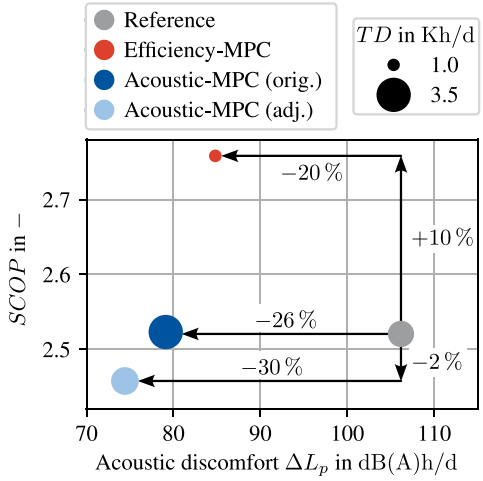


Fig. 14. Comparison of the $SCOP$, acoustic discomfort ΔL_p and thermal discomfort TD (given by the size of the dots) for placement scenario 2. The original Acoustic-MPC (developed for placement scenario 1) already decreases the acoustic discomfort by 26%. By further tuning the cost function weights for placement scenario 2 we obtain a reduction of 30% compared to the reference controller.

increases throughout the day and reaches its maximum at 10 p.m. before decreasing until 6 a.m. by an average of 9 K. In comparison to the other MPC configurations, the storage temperature reaches a higher maximum temperature at 10 p.m. to minimize heat pump operation during the night. Towards the end of the night, part-load operation occurs at constant compressor speed if necessary. The temperature is lower at 6 a.m., resulting in a higher thermal discomfort during the night. High noise levels are recorded after 6 a.m. and towards the evening as the heat pump operates at full speed to raise storage temperatures. The buffer storage temperature decreases around 2 p.m. due to solar radiation.

Fig. 14 presents a comparison of KPIs, while Table 5 provides the absolute values. Due to the reduced distance from the building, sound pressure levels are higher, leading to a significant increase in acoustic discomfort compared to placement scenario 1 (Fig. 12).

In terms of acoustic discomfort, the reference scenario records 106.2 dB(A)h/d, while Efficiency-MPC shows a reduction to 84.8 dB(A)h/d (−20%).

The original Acoustic-MPC configuration reaches the same $SCOP$ as the reference controller. With loading the buffer storage before 10 p.m., a reduction of 26% in acoustic discomfort compared to the reference controller and 6% compared to the Efficiency-MPC is reached. The thermal discomfort increases to 3.5 Kh/d (mainly around 6 a.m.).

For the adjusted Acoustic-MPC, the buffer storage temperature is increased even stronger towards 10 p.m. leading in a 2% decrease in $SCOP$. The high buffer storage temperatures allow a higher reduction in acoustic discomfort when comparing Acoustic-MPC to the reference controller — specifically a decrease of 30% from 106.2 dB(A)h/d to 84.8 dB(A)h/d. Thermal discomfort increases slightly by 0.2 Kh/d compared to the reference controller but can be improved by more than 1 Kh/d compared to the original Acoustic-MPC configuration.

6. Discussion

The presented study successfully demonstrates that a multi-objective MPC can enhance energy efficiency and reduce noise emissions in ASHPs. The Efficiency-MPC improved $SCOP$ by up to 10%, while the Acoustic-MPC reduced acoustic discomfort by 92% through strategic load shifting. Both configurations maintained thermal comfort and demonstrated robustness across different placement scenarios, highlighting the potential of MPC to optimize ASHP operation for real-world applications. Additionally, we evaluated the robustness of cost function weights across different placement scenarios. While fine-tuning the weights can provide minor improvements, the results obtained with non-tuned weights indicate that the MPC is relatively insensitive to changes in placement, which is critical for practical applications where re-optimization for every unique scenario is infeasible. The cost function weights were determined through sensitivity analysis, providing a balanced trade-off between competing objectives. Since noise perception is inherently subjective, the trade-off between energy efficiency and noise emission reduction can vary significantly based on individual user preferences. In practice, users could adjust the weights in the MPC cost function to align with their specific needs. For example, users particularly sensitive to noise could increase the penalization of sound pressure levels to prioritize noise reduction.

While the results of the study are promising, there are open research questions and limitations to address before the presented controller can be applied in the field. These limitations are discussed in the following:

Table 5
KPIs of the simulations at proximal installation (placement scenario 2).

KPI & Unit	Reference	Efficiency-MPC	Acoustic-MPC	
			Original weights	Adjusted weights
$SCOP$ in –	2.52	**2.76**	2.52	2.46
Acoustic discomfort ΔL_p in dB(A)h/d	106.2	84.8	79.1	**74.4**
Thermal discomfort TD in Kh/d	2.28	**1.01**	3.50	2.47
Average compressor starts n_{Starts} in 1/d	**2.10**	36.9	4.26	4.48
Average buffer storage temperature in °C	38.7	**30.6**	36.28	38.5

- **Building energy system model**: While our study demonstrated the feasibility of multi-objective control optimization under dynamic operation, the simplified configuration of our building energy system (single thermal zone, no domestic hot water) limits the complexity compared to real-world systems. While linear models have been successfully employed in the literature for controlling room temperatures in real buildings [55], more complex models may be necessary for managing energy systems with greater complexity than addressed in this study. Consequently, future research should validate the applicability of this approach in more intricate real-world scenarios.
- **Perfect forecasts**: Our presented approach assumes that external variables are known with certainty. However, uncertainties in these variables can significantly influence the performance of MPC [62]. Future work should consider incorporating uncertainty analysis to better predict real-world performance.
- **Computational complexity**: The limited computational resources of ASHP microcontrollers make local MPC evaluation challenging. Cloud computing presents a promising solution to address these limitations [63,64]; however, successful, and fail-safe implementations still need thorough investigation.
- **Psychoacoustics**: A notable finding is that applying MPC led to frequent compressor starts, resulting in fluctuating technical noise, often perceived as unpleasant by occupants [65]. Understanding human perception of these noises remains ongoing research [66]. Future studies should move beyond using sound pressure levels as optimization metrics; instead, psychoacoustic KPIs such as loudness, sharpness, and fluctuation strength could more accurately reflect human auditory experience and help to reduce perceived discomfort, ultimately decreasing disturbances.
- **Impact of Aging**: In practice, long-term operation can result in reduced energy efficiency and increased noise emissions due to the aging of system components. These changes may cause the process models to deviate from real-world performance over time. Online learning can be implemented to periodically update the process models using monitoring data. While this is feasible for the power consumption process model, adjusting the noise emission process model in real-world applications is impractical, as it requires direct acoustic measurements of the ASHP. A practical alternative is the inclusion of a user input loop, which allows the user to directly adjust cost function weight parameters based on perceived noise levels.

7. Conclusion

In this study, we present a novel data-driven Model Predictive Control (MPC) approach to optimize the operation of a heat pump system with respect to energy efficiency and noise emissions. The MPC controls the compressor speed and the heating circuit valve of a building energy system model. The model includes a thermodynamically and acoustically validated heat pump, buffer storage, underfloor heating, and the building itself. Data-driven process models (linear regression, grey-box) predict system variables, such as zone temperature, buffer storage temperature, and heat pump power consumption. These models are trained using 30 days of operational data sampled from a reference controller. Two MPC configurations are investigated, which differ in cost function weights to prioritize either efficiency (Efficiency-MPC) or noise reduction (Acoustic-MPC). The cost function weights are determined through a sensitivity study. The MPC's are tested for two ASHP placement scenarios — distal and proximal installation — which results in different sound levels at immission.

The Efficiency-MPC improves efficiency compared to a state-of-the-art reference controller by 10% by exploiting its knowledge on future internal gains and solar radiation. Additionally, the controller reduces the supply temperature compared to the reference controller, which significantly lowers noise emissions by up to 20%. This is because a reduced supply temperature leads to a lower power consumption, resulting in a decreased acoustic discomfort.

The Acoustic-MPC reduced the acoustic discomfort compared to the reference controller and Efficiency-MPC. For distal installations, MPC-Acoustic obtains a significant reduction in acoustic discomfort by –92%, along with a 6% increase in $SCOP$ compared to the reference controller. The decrease in acoustic discomfort is reached by strategically utilizing system flexibility to shift heat pump operation to daytime, where higher acoustic limits are permitted. For proximal installation, the Acoustic-MPC reduces acoustic discomfort by 26% compared to the reference controller, achieving a similar $SCOP$ even without fine-tuning the cost function weights for the changed placement. With fine-tuned weights, the Acoustic-MPC achieves a slightly greater reduction in acoustic discomfort (30% compared to the reference) at the cost of a minor decrease in $SCOP$ decrease of 2%. In general, proximal installation demonstrated less potential for noise reduction, as the noise limits are exceeded even on part-load operation leaving less margin for a reduction in acoustic discomfort.

By comparing two Acoustic-MPC configurations — each with cost function weights optimized for different placement scenarios — we evaluate the transferability of the MPC approach to various installation contexts. Our results demonstrate that the cost function weights are not sensitive to changes in heat pump placement, indicating that the MPC configurations can be effectively applied across different scenarios without significant re-tuning.

Overall, this study demonstrates the effectiveness of data-driven model predictive control in simultaneously enhancing energy efficiency and reducing acoustic emissions of ASHP while maintaining thermal comfort. Future research could focus on validating these findings through real-world experiments.

Declaration of generative AI and AI-assisted technologies in the writing process

We utilized RWTHgpt, an AI language model developed by OpenAI, to generate initial drafts based on our input. The generated text was subsequently reviewed and edited to align with our research objectives and standards.

Declaration of competing interest

The authors declare that they have no known competing financial interests or personal relationships that could have appeared to influence the work reported in this paper.

Table A.6
Models used to describe the building energy system.

Model	Relevant parameters		Model path	Source
	Parameter	Value		
Building	Living Area	130 m²	`BESMod.Systems.Demand.Building`	Wüllhorst et al. [41]
	Number of floors	1	`.TEASERThermalZone`	
	Height of floors	2.5 m	The nominal heating load of the building is calculated in	
	Nominal heating load	6.6 kW	accordance with DIN EN 12831 [67].	
	Nom. ambient temperature	−12 °C		
	Nom. supply temperature	45 °C		
	Thermal zones	1		
Transfer system			`BESMod.Systems.Hydraulical.Transfer` `.UFHTransferSystem`	Wüllhorst et al. [41]
Underfloor heating	Floor or Ceiling	Floor	`BESMod.Systems.Hydraulical.Components`	Wüllhorst et al. [41]
	Heat convection model	EN ISO 6946	`.UFH.PanelHeating`	
Pumps			`IBPSA.Fluid.Movers.SpeedControlled_y`	Wetter et al. [45]
Valve			`AixLib.Fluid.Actuators.Valves` `.TwoWayEqualPercentage`	Maier et al. [47]
Distribution system	use_dhw	False	`BESMod.Systems.Hydraulical.Distribution` `.DistributionTwoStorageParallel` (DHW storage and associated models are removed)	Wüllhorst et al. [41]
Buffer storage	Volume	7841	`AixLib.Fluid.Storage.Storage`	Maier et al. [47]
	dTLoadingHC1	5 K		
	Number of layers	4		
Generation system			`BESMod.Systems.Hydraulical.Generation` `.HeatPumpAndHeatingRod`	Wüllhorst et al. [41]
Heat pump	Design type	Monovalent	`AixLib.Fluid.HeatPumps.HeatPump`	Wüllhorst et al. [48]
	Performance data	Tables A.8 to A.13		

Acknowledgment

We gratefully acknowledge the financial support by the German Federal Ministry for Economic Affairs and Climate Action (BMWK), promotional reference 03EN4020A.

Appendix A. Modeling of the building energy system

Table A.7
Libraries used in Modelica.

Library	Software version	Source
`AixLib`	1.3.1	[47]
`BESMod`	0.3.1	[41]
`BuildingSystems`	2.0.0-beta	[42]
`Buildings`	12.0.0	[43]
`IDEAS`	3.0.0	[44]
`IBPSA`	4.0.1	[45]
`TEASER`	1.1.0	[46]

Table A.8
Electrical power consumption P_{el} of the heat pump at a compressor speed of u_{Comp} = 30 Hz.

P_{el}, u_{Comp} = 30 Hz		Ambient temperature		
		−7 °C	0 °C	12 °C
Supply temperature	35 °C	1.07 kW	1.00 kW	0.82 kW
	45 °C	1.19 kW	1.27 kW	1.15 kW
	55 °C	1.30 kW	1.43 kW	1.50 kW

Table A.9
Electrical power consumption P_{el} of the heat pump at a compressor speed of u_{Comp} = 55 Hz.

P_{el}, u_{Comp} = 55 Hz		Ambient temperature		
		−7 °C	0 °C	12 °C
Supply temperature	35 °C	1.89 kW	1.94 kW	1.60 kW
	45 °C	2.03 kW	2.21 kW	2.06 kW
	55 °C	2.30 kW	2.45 kW	2.42 kW

Table A.10
Electrical power consumption P_{el} of the heat pump at a compressor speed of u_{Comp} = 81 Hz.

P_{el}, u_{Comp} = 81 Hz		Ambient temperature		
		−7 °C	0 °C	12 °C
Supply temperature	35 °C	2.47 kW	2.42 kW	2.96 kW
	45 °C	2.77 kW	2.91 kW	2.65 kW
	55 °C	3.29 kW	3.39 kW	3.28 kW

Table A.11
Condenser power $\dot{Q}_{Cond}$ of the heat pump at a compressor speed of u_{Comp} = 30 Hz.

$\dot{Q}_{Cond}$, u_{Comp} = 30 Hz		Ambient temperature		
		−7 °C	0 °C	12 °C
Supply temperature	35 °C	3.36 kW	3.78 kW	4.67 kW
	45 °C	3.12 kW	3.83 kW	4.75 kW
	55 °C	2.95 kW	3.63 kW	4.88 kW

Table A.12
Condenser power $\dot{Q}_{Cond}$ of the heat pump at a compressor speed of u_{Comp} = 55 Hz.

$\dot{Q}_{Cond}$, u_{Comp} = 55 Hz		Ambient temperature		
		−7 °C	0 °C	12 °C
Supply temperature	35 °C	5.91 kW	7.30 kW	9.18 kW
	45 °C	5.32 kW	6.69 kW	8.47 kW
	55 °C	5.20 kW	6.23 kW	7.89 kW

Table A.13
Condenser power $\dot{Q}_{Cond}$ of the heat pump at a compressor speed of u_{Comp} = 81 Hz.

$\dot{Q}_{Cond}$, u_{Comp} = 81 Hz		Ambient temperature		
		−7 °C	0 °C	12 °C
Supply temperature	35 °C	7.73 kW	9.09 kW	11.20 kW
	45 °C	7.23 kW	8.79 kW	10.91 kW
	55 °C	7.43 kW	8.64 kW	10.71 kW

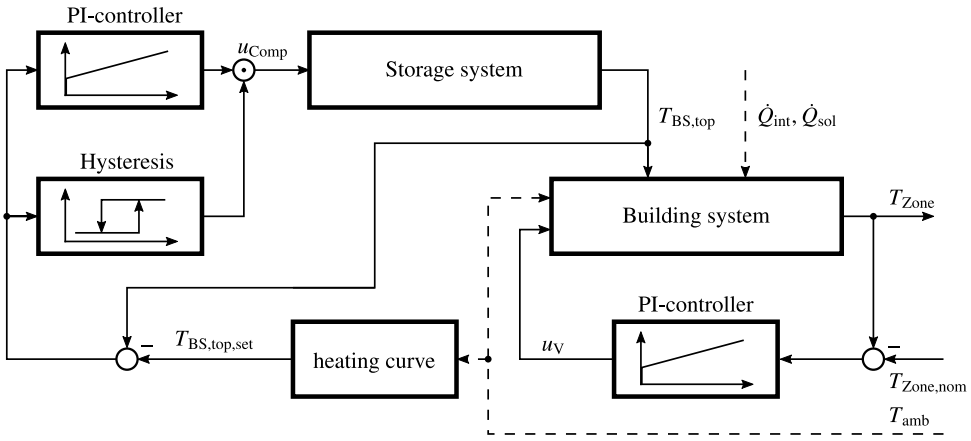


Fig. A.15. Flow chart of the reference controller. Disturbances (ambient temperature T_{amb}, internal gains $\dot{Q}_{int}$ and solar radiation $\dot{Q}_{sol}$) are indicated by dashed lines.

Table A.14
Parameters of the reference controller.

(a) PI controller and hysteresis.			(b) Heating curve.	
Parameter	Compressor	Valve	Parameter	Value
Proportional term K_P	0.045	0.9	Standard ambient temperature $T_{amb,std}$	−12 °C
Integral term t_I	600	1000	Nominal storage temperature $T_{BS,nom}$	45 °C
Bandwidth	5 K	–	Nominal zone temperature $T_{Zone,nom}$	20 °C
			Exponent heating curve n	1
			Summand heating curve ΔT_{BS}	5 K

The command variable of the buffer storage temperature $T_{BS,top,set}$ is calculated by the heating curve for the reference controller based on Eq. (A.1). Since we did not apply changes to the building model from the BESMod, the parameters of the heating curve remain unchanged [41]. Only the summand ΔT_{BS} is added to increase the temperature due to temperature losses in the storage. The value is equal to the nominal temperature difference in the buffer storage (dtLoadingHC1 in Table A.8).

$$T_{BS,top,set} = (T_{BS,top,nom} - T_{Zone,nom}) \cdot \left(\frac{T_{Zone,nom} - T_{amb}}{T_{Zone,nom} - T_{amb,std}} \right)^{\frac{1}{n}} + T_{Zone,nom} + \Delta T_{BS} \tag{A.1}$$

The PI controllers are implemented for every time step k according to Eqs. (A.2) and (A.7) respectively. The proportional and integral terms of both controllers are given in Table A.14a. The Anti Windup correlation was implemented by Stoffel et al. [55] and is used for both PI controllers. The compressor speed applied to the system is also dependent on the hysteresis.

$$u_{V,k} = \min\left(\max\left(0, K_{P,V} \cdot \left(e_{Zone,n} + \frac{i_{Zone,k}}{t_{I,V}} \right) \right), 1 \right) \tag{A.2}$$

$$e_{Zone,k} = T_{Zone,k} - T_{Zone,nom,k} \tag{A.3}$$

$$i_{Zone,k} = \underbrace{\frac{i_{Zone,k-1}}{K_{P,V}} - e_{Zone,k-1}}_{\text{Anti-Windup}} + \underbrace{\frac{1}{t_{I,V} \cdot e_{Zone,k} \cdot \Delta t_k}}_{\text{Integral}} \tag{A.4}$$

$$u_{Comp,PI,k} = \min\left(\max\left(0, K_{P,Comp} \cdot \left(e_{BS,top,n} + \frac{i_{BS,top,k}}{t_{I,Comp}} \right) \right), 1 \right) \tag{A.5}$$

$$e_{BS,top,k} = T_{BS,top,k} - T_{BS,top,set,k} \tag{A.6}$$

$$i_{BS,top,k} = i_{BS,top,k} = \underbrace{\frac{i_{BS,top,k-1}}{K_{P,Comp}} - e_{BS,top,k-1}}_{\text{Anti-Windup}} + \underbrace{\frac{1}{t_{I,Comp} \cdot e_{BS,top,k} \cdot \Delta t_k}}_{\text{Integral}} \tag{A.7}$$

Table A.15
Parameters of the cost function.

Parameter	Value
$P_{el,max}$	4.5 kW
$u_{Comp,min}$	0
$u_{Comp,max}$	1
$u_{V,min}$	0.02
$u_{V,max}$	1
$T_{BS,top,min}$	20 °C
$T_{BS,top,max}$	60 °C

Appendix B. Data generation for process model training

The generation of training data involves four distinct control configurations. Initially, the system operates according to a previously established control concept, where set temperatures for the buffer storage are randomized to cover the entire operational range. This approach allows process models to learn various behaviors without relying solely on predefined heating curves. The first dataset captures this operation, while subsequent datasets include variations such as turning off the compressor or closing the valve for specified duration.

In total, four datasets are generated:

- **Mode 1**: Randomized set temperatures for both buffer storage and zone temperature (one week in January, February and March respectively). The reference controller from Section 4 is used here.
- **Mode 2**: Features a reversed control operation where buffer storage temperature is regulated by valve opening and zone temperature by compressor speed (one week in January, February and March respectively). This approach is not suitable regular operation because it leads to significant control deviations for the zone temperature.
- **Mode 3**: Involves shutting down the compressor for one day and one day in mode 1 respectively (eight days in February).
- **Mode 4**: Involves setting the valve opening degree to its minimum for one day and one day in mode 1 respectively (eight days in February).

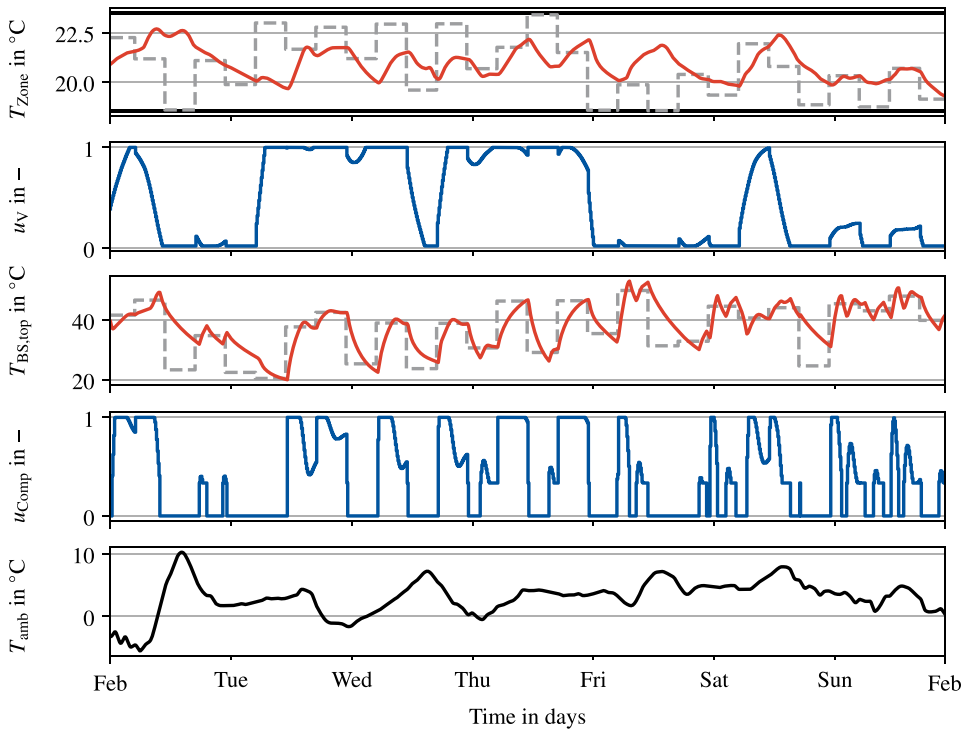
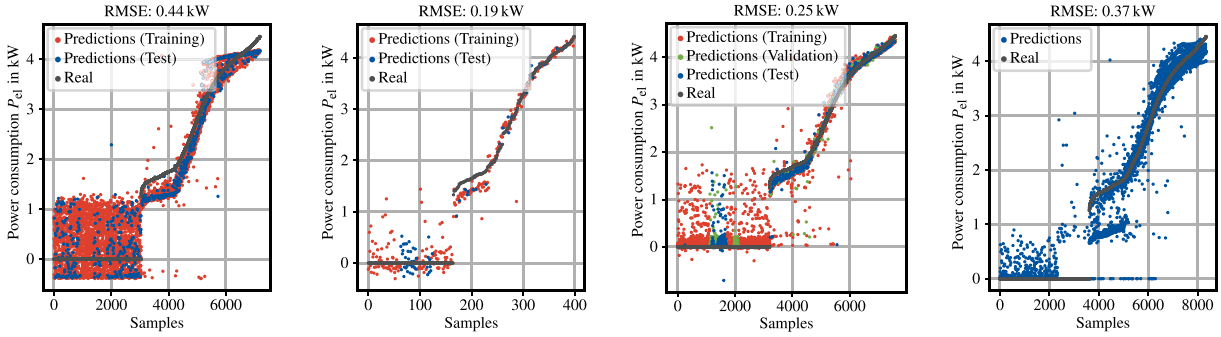
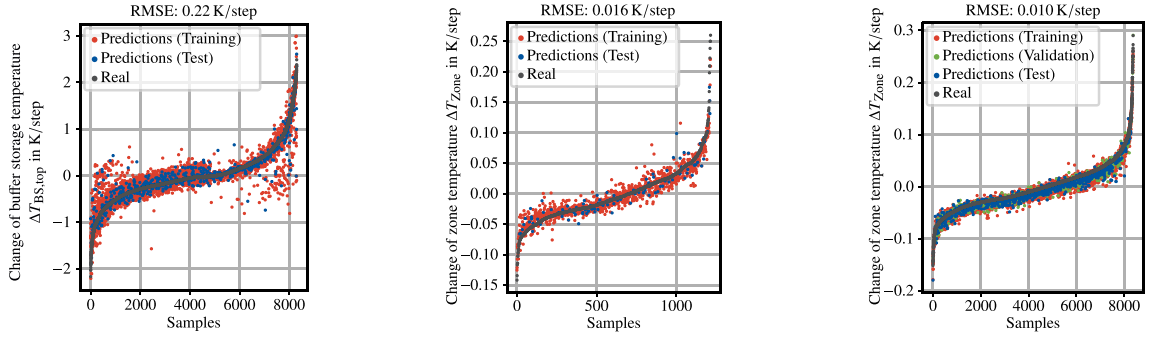


Fig. B.16. One week of training data in mode 1 in February. The control values are plotted in red, command values in grey and manipulated values in blue.



(a) Linear regression. (b) Gauss-process model. (c) Artificial Neural Network. (d) Grey-Box model.

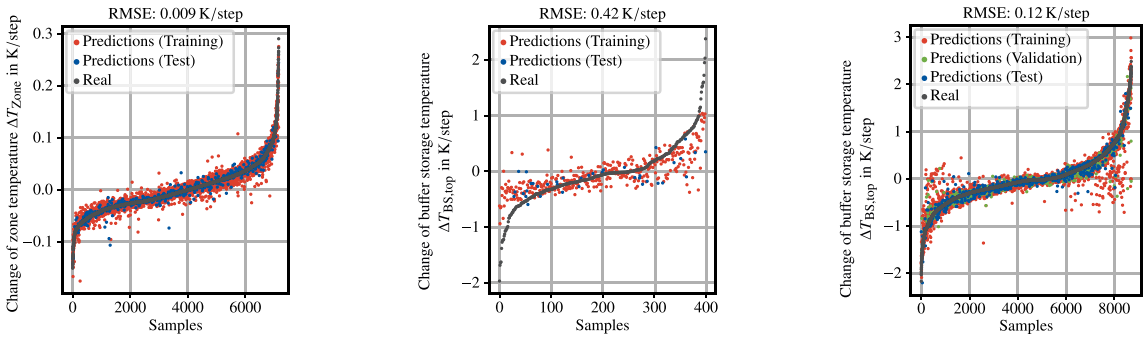
Fig. C.17. Comparison of the process models of the heat pumps power consumption.



(a) Linear regression. (b) Gauss-process model. (c) Artificial Neural Network.

Fig. C.18. Comparison of the process models predicting the change of zone temperature.

Fig. B.16 displays the zone temperature T_{Zone}, the valve opening u_V, the buffer storage temperature $T_{BS,top}$, the compressor speed u_{Comp} and the ambient temperature T_{amb} for mode 1 throughout the interval in February. The command values are selected randomly for an interval



(a) Linear regression. (b) Gauss-process model. (c) Artificial Neural Network.

Fig. C.19. Comparison of the process models predicting the change of buffer storage temperature.

of six hours between 18.5 °C and 23.5 °C for the zone temperature and 20 °C and 50 °C for the buffer storage temperature.

Appendix C. Process model training

The following figures show the results of the model training. The data generated based on the four modes in Appendix C are split randomly into up to three parts based on the model type. Linear regressions and GPR require training and test data. To reach a satisfactory accuracy of the models we use 80% of the data for training and 20% for testing. The data for ANN is split into 60% for training, 20% for validation, and 20% for testing [55]. The parameters of the grey-box model (Fig. C.17(c)) are empirically optimized through iterative testing. We systematically adjusted coefficient values and evaluated the model's performance with the RMSE. This process was repeated until a satisfactory level of accuracy was achieved (see Figs. C.18 and C.19).

Appendix D. Sensitivity analysis

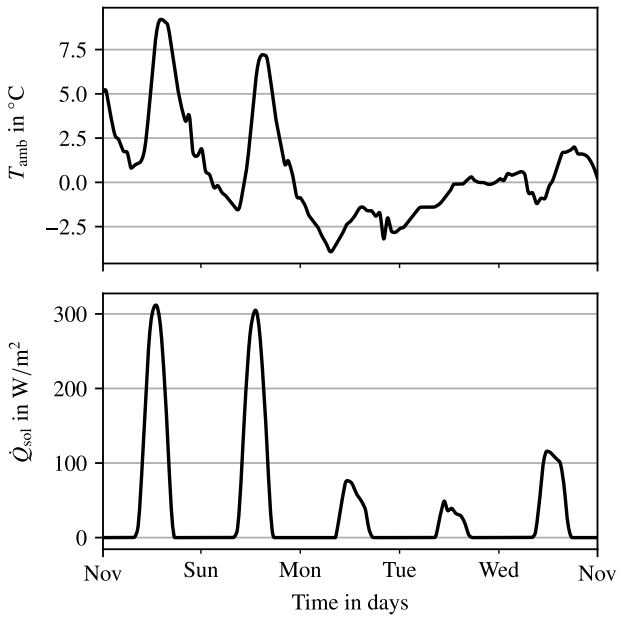


Fig. D.20. Ambient temperature and solar radiation during the five analyzed days of the sensitivity analysis.

Data availability

Data will be made available on request.

Table D.16
Tested weights in sensitivity analysis for every MPC scenario. The values were selected based on expert knowledge.

Scenario	Weight	Values
Efficiency-MPC	$w_{T_{Zone}}$	1
	$w_{P_{el}}$	0.03; 0.1; 0.3; 1; 3
	$w_{T_{BS,top}}$	0; 0.01; 0.03; 0.1
Acoustic-MPC, Placement Scenario 1	$w_{T_{Zone}}$	1
	w_{L_p}	1; 3; 10; 30; 100
	$w_{P_{el}}$	0.003; 0.001; 0.03; 0.1; 0.3
	w_{u_V}	0; 0.001; 0.01
Acoustic-MPC, Placement Scenario 2	$w_{T_{Zone}}$	1
	w_{L_p}	0.3; 1; 3; 10; 30
	$w_{P_{el}}$	0.03; 0.1; 0.3; 1; 3
	w_{u_V}	0; 0.001; 0.01

References

[1] T. Nowak, P. Westring, European Heat Pump Market and Statistics Report 2023, European Heat Pump Association, Brussels, Belgium, 2023.

[2] F. Alshehri, S. Beck, D. Ingham, L. Ma, M. Pourkashanian, Techno-economic analysis of ground and air source heat pumps in hot dry climates, J. Build. Eng. 26 (2019) 100825, http://dx.doi.org/10.1016/j.jobe.2019.100825, URL https://linkinghub.elsevier.com/retrieve/pii/S2352710219302001.

[3] D. Romanov, B. Leiss, Geothermal energy at different depths for district heating and cooling of existing and future building stock, Renew. Sustain. Energy Rev. 167 (2022) 112727, http://dx.doi.org/10.1016/j.rser.2022.112727, URL https://www.sciencedirect.com/science/article/pii/S1364032122006165.

[4] W. Beentjes, T. Campmans, Dutch building code regulates noise limits for outside placed heat pumps, INTER- NOISE NOISE- CON Congr. Conf. Proc. 263 (5) (2021) 1703–1711, http://dx.doi.org/10.3397/IN-2021-1904.

[5] E.H.P. Association, White paper: Heat pumps and sound, 2020, URL https://www.ehpa.org/news-and-resources/publications/white-paper-heat-pumps-and-sound/.

[6] C. Reichl, IEA HPT annex63: Placement impact on heat pump acoustics, 2023, URL https://heatpumpingtechnologies.org/annex63/.

[7] X. Zhang, Y. Hu, S. Geng, Q. Hu, H. Wang, Research on noise reduction scheme of heat pump unit in a square, J. Chem. 2020 (2020) 1–6, http://dx.doi.org/10.1155/2020/1237034, URL https://consensus.app/papers/research-noise-reduction-scheme-heat-pump-unit-square-zhang/3d79b4fd3a745fe8ba91603ceb46f755/.

[8] H. Hellgren, O. Gustafsson, P. Bergman, Improved measurement method for heat pump noise, Heat Pump Conf. Rotterdam (2017) 5, 00000.

[9] M. Flimel, The assessment of noise generated by heat pumps installed outdoors, Akustika (2020) http://dx.doi.org/10.36336/akustika2020372, URL https://consensus.app/papers/assessment-noise-generated-heat-pumps-installed-outdoors-flimel/0faa6286ceb95e68a992736f4af02719/.

[10] C. Feldmann, T. Carolus, M. Schneider, Psychoacoustical investigation of sounds from heat pumps, in: International Conference on Fan Noise, Aerodynamics, Applications and System, Darmstadt, 2018, p. 12, URL https://www.fan2022.org/archives/fan2018/papers/paper-11.html.

[11] T. Zhu, T.H. Carolus, Axial fan tip clearance noise: Experiments, Lattice–Boltzmann simulation, and mitigation measures, Int. J. Aeroacoustics 17 (1–2) (2018) 159–183, http://dx.doi.org/10.1177/1475472X17743627, URL http://journals.sagepub.com/doi/10.1177/1475472X17743627.

[12] E. Envia, Fan noise reduction: An overview, Int. J. Aeroacoustics 1 (1) (2002) 43–64, 36 citations (Crossref) [2021-03-08]. doi: 10/d6ngzp. URL http://journals.sagepub.com/doi/10.1260/1475472021502668.

[13] A. Lucius, M. Schneider, S.S.-D. Bortoli, T. Gerhard, T. Geyer, Aeroacoustic simulation and experimental validation of sound emission of an axial fan applied in a heat pump, in: PROCEEDINGS of the 23rd International Congress on Acoustics, Aachen, Germany, 2019, pp. 1851–1858.

[14] F. Czwielong, S. Becker, Impact of heat exchangers on axial fan rotor noise in heat pump applications, in: Proceedings of the 10th Convention of the European Acoustics Association Forum Acusticum 2023, European Acoustics Association, Turin, Italy, 2024, pp. 3885–3892, http://dx.doi.org/10.61782/fa.2023.0788, URL https://dael.euracoustics.org/confs/landing_pages/fa2023/000788.html.

[15] F. Czwielong, S. Floss, M. Kaltenbacher, S. Becker, Sound reduction in heat exchanger modules by integrating plate absorbers with sub-millimeter openings, Acta Acust. 5 (2021) 35, http://dx.doi.org/10.1051/aacus/2021020, URL https://acta-acustica.edpsciences.org/10.1051/aacus/2021020.

[16] O. Gustafsson, C. Haglund Stignor, J.-O. Dalenbäck, Heat exchanger design aspects related to noise in heat pump applications, Appl. Therm. Eng. 93 (2016) 742–749, http://dx.doi.org/10.1016/j.applthermaleng.2015.10.057, URL https://linkinghub.elsevier.com/retrieve/pii/S1359431115011047.

[17] J. Park, S. Wang, Noise reduction for compressors by modes control using topology optimization of eigenvalue, J. Sound Vib. 315 (4–5) (2008) 836–848, http://dx.doi.org/10.1016/j.jsv.2008.01.064, URL https://linkinghub.elsevier.com/retrieve/pii/S0022460X08001156.

[18] N. Rahmani, Y. Khastavan, A.S. Variani, S. Ahmadi, Compressor pulsation noise attenuation using reactive silencer with various configurations: A theoretical and experimental study, Heliyon 10 (5) (2024) e27263, http://dx.doi.org/10.1016/j.heliyon.2024.e27263, URL https://linkinghub.elsevier.com/retrieve/pii/S2405844024032948.

[19] H. Wang, Z. Xie, Y. Lu, W. Chu, Z. Li, Research on noise reduction of variable speed rotary compressor with large capacity, in: International Compressor Engineering Conference, in: Paper 2655, 2020, p. 7.

[20] M. Silveira, F. Fagotti, Noise reduction of commercial applications: compressor approach, in: International Compressor Engineering Conference, in: Paper 1759, 2006, p. 8.

[21] D. Liu, Y. Feng, J. Jia, P. Si, Y. Feng, The noise spectral characteristics and noise reduction schemes of screw air-source heat pump: A case study, Build. Simul. 17 (1) (2024) 53–70, http://dx.doi.org/10.1007/s12273-023-1085-2, URL https://link.springer.com/10.1007/s12273-023-1085-2.

[22] T. Gindre, T. Oltersdorf, C. Vering, J. Emhofer, C. Reichl, K. Arumugam, Final report - part 10 annex 51: Acoustic signatures of heat pumps, 2021, URL https://heatpumpingtechnologies.org/publications/final-report-part-10-annex-51-acoustic-signatures-of-heat-pumps/.

[23] N.E. Systems, Users manual - NIBE air/water heat pump F2120 8, 12 – 2x230V, 2020.

[24] M.H.I. thermal Systems. Ltd., Users manual - mitsubishi electric - remote control RC-EX3, 2017, URL https://www.mhi-mth.co.jp/en/products/pdf/pjz012a160_english.pdf.

[25] C. Vering, J. Klingebiel, C. Reichl, J. Emhofer, M. Nürenberg, D. Müller, Simultaneous energy efficiency and acoustic evaluation of heat pump systems using dynamic simulation models, in: 13th IEA Heat Pump Conference 2021 Cenference Proceedings - Full Papers, IEA Heat Pumping Technologies, Jeju, Korea, 2020, pp. 393–403.

[26] P. Stoffel, L. Maier, A. Kümpel, T. Schreiber, D. Müller, Evaluation of advanced control strategies for building energy systems, Energy Build. 280 (2023) 112709, http://dx.doi.org/10.1016/j.enbuild.2022.112709, URL https://www.sciencedirect.com/science/article/pii/S0378778822008805.

[27] A. Mugnini, M. Evens, A. Arteconi, Model predictive controls for residential buildings with heat pumps: Experimentally validated archetypes to simplify the large-scale application, Energy Build. 320 (2024) 114632, http://dx.doi.org/10.1016/j.enbuild.2024.114632, URL https://www.sciencedirect.com/science/article/pii/S0378778824007485.

[28] S. Kuboth, F. Heberle, T. Weith, M. Welzl, A. König-Haagen, D. Brüggemann, Experimental short-term investigation of model predictive heat pump control in residential buildings, Energy Build. 204 (2019) 109444, http://dx.doi.org/10.1016/j.enbuild.2019.109444, URL https://www.sciencedirect.com/science/article/pii/S0378778819320419.

[29] S. Steinle, M. Zimmerlin, F. Mueller, L. Held, M. Suriyah, T. Leibfried, Time-dependent flexibility potential of heat pump systems for smart energy system operation, Energies (2020) http://dx.doi.org/10.3390/en13040903, URL https://consensus.app/papers/timedependent-flexibility-potential-heat-pump-systems-steinle/dc5821a20e2357c69214ac004adabca5/.

[30] T.Q. Péan, J. Salom, R. Costa-Castelló, Review of control strategies for improving the energy flexibility provided by heat pump systems in buildings, Efficient energy management, J. Process Control 74 (2019) 35–49, http://dx.doi.org/10.1016/j.jprocont.2018.03.006, URL https://www.sciencedirect.com/science/article/pii/S0959152418300489.

[31] G. Serale, M. Fiorentini, A. Capozzoli, D. Bernardini, A. Bemporad, Model predictive control (MPC) for enhancing building and HVAC system energy efficiency: Problem formulation, applications and opportunities, Energies 11 (3) (2018) 631, http://dx.doi.org/10.3390/en11030631, URL https://www.mdpi.com/1996-1073/11/3/631.

[32] B. Yue, B. Su, F. Xiao, A. Li, K. Li, S. Li, R. Yan, Q. Lian, A. Li, Y. Li, X. Fang, X. Liang, Energy-oriented control retrofit for existing HVAC system adopting data-driven MPC – methodology, implementation and field test, Energy Build. 295 (2023) 113286, http://dx.doi.org/10.1016/j.enbuild.2023.113286, URL https://www.sciencedirect.com/science/article/pii/S0378778823005169.

[33] D. Atabay, Comparison of Optimization Methods for Model Predictive Control: An Application to a Compressed Air Energy Storage System (Dissertation), Technischen Universität München, Munich, Germany, 2017.

[34] B.V. Mbuwir, D. Geysen, G. Kosmadakis, M. Pilou, G. Meramveliotakis, H. Toersche, Optimal control of a heat pump-based energy system for space heating and hot water provision in buildings: Results from a field test, Energy Build. 310 (2024) 114116, http://dx.doi.org/10.1016/j.enbuild.2024.114116, URL https://linkinghub.elsevier.com/retrieve/pii/S0378778824002329.

[35] P. Stoffel, C. Loffler, S. Eser, A. Kumpel, D. Muller, Combining data-driven and physics-based process models for hybrid model predictive control of building energy systems, in: 2022 30th Mediterranean Conference on Control and Automation, MED, IEEE, Vouliagmeni, Greece, 2022, pp. 121–126, http://dx.doi.org/10.1109/MED54222.2022.9837277, URL https://ieeexplore.ieee.org/document/9837277/.

[36] S. Göbel, P. Stoffel, F. Will, C. Vering, D. Müller, Maximizing operational efficiency of heat pumps with model predictive control: An experimental case study for residential application, in: 14th IEA Heat Pump Conference 2023 (HPC2023) Conference Proceedings – Full Papers, Chicago, IL, USA, 2023, p. 12, URL https://heatpumpingtechnologies.org/publications/presentation-no-805-maximizing-operational-efficiency-of-heat-pumps-withmodel-predictive-control-an-experimental-case-study-for-residential-application-14th-iea-heat-pump-conference-chicago/.

[37] W. Wang, B. Hu, R. Wang, M. Luo, G. Zhang, B. Xiang, Model predictive control for the performance improvement of air source heat pump heating system via variable water temperature difference, Int. J. Refrig. 138 (2022) 169–179, http://dx.doi.org/10.1016/j.ijrefrig.2022.03.001, URL https://www.sciencedirect.com/science/article/pii/S0140700722000548.

[38] V. Klepic, M. Wolf, T. Pröll, Extension of a low-tech model predictive control (MPC) algorithm for grid-supportive heat pump operation, Energy Build. 323 (2024) 114733, http://dx.doi.org/10.1016/j.enbuild.2024.114733, URL https://www.sciencedirect.com/science/article/pii/S0378778824008491.

[39] F. Bünning, J. Warrington, P. Heer, R.S. Smith, J. Lygeros, Robust MPC with data-driven demand forecasting for frequency regulation with heat pumps, Control Eng. Pract. 122 (2022) 105101, http://dx.doi.org/10.1016/j.conengprac.2022.105101, URL https://www.sciencedirect.com/science/article/pii/S0967066122000247.

[40] J. Prášek, P. Trnka, V. Havlena, P. McGahan, Range control MPC with application to vapor compression cycles, Control Eng. Pract. 96 (2020) 104309, http://dx.doi.org/10.1016/j.conengprac.2020.104309, URL https://www.sciencedirect.com/science/article/pii/S0967066120300071.

[41] F. Wüllhorst, L. Maier, D. Jansen, L. Kühn, D. Hering, BESMod - a modelica library providing building energy system modules, in: Proceedings of the American Modelica Conference 2022, Dallas, TX, US, 2022, pp. 9–18, http://dx.doi.org/10.3384/ECP211869.

[42] C. Nytsch-Geusen, J. Huber, M. Ljubijankic, J. Rädler, Modelica building systems - eine modellbibliothek zur simulation komplexer energietechnischer Gebäudesysteme, Bauphysik 35 (1) (2013) 21–29, http://dx.doi.org/10.1002/bapi.201310045, URL https://onlinelibrary.wiley.com/doi/10.1002/bapi.201310045.

[43] M. Wetter, W. Zuo, T.S. Nouidui, X. Pang, Modelica buildings library, J. Build. Perform. Simul. 7 (4) (2014) 253–270, http://dx.doi.org/10.1080/19401493.2013.765506, URL http://www.tandfonline.com/doi/abs/10.1080/19401493.2013.765506.

[44] F. Jorissen, G. Reynders, R. Baetens, D. Picard, D. Saelens, L. Helsen, Implementation and verification of the IDEAS building energy simulation library, J. Build. Perform. Simul. 11 (6) (2018) 669–688, http://dx.doi.org/10.1080/19401493.2018.1428361, URL https://www.tandfonline.com/doi/full/10.1080/19401493.2018.1428361.

[45] M. Wetter, D. Blum, J. Hu, Modelica IBPSA library, 2019, URL https://www.osti.gov/doecode/biblio/25252.

[46] P. Remmen, M. Lauster, M. Mans, M. Fuchs, T. Osterhage, D. Müller, TEASER: An open tool for urban energy modelling of building stocks, J. Build. Perform. Simul. 11 (1) (2018) 84–98, http://dx.doi.org/10.1080/19401493.2017.1283539.

[47] L. Maier, D. Jansen, F. Wüllhorst, M. Kremer, A. Kümpel, T. Blacha, D. Müller, AixLib: An open-source Modelica library for compound building energy systems from component to district level with automated quality management, J. Build. Perform. Simul. (2023) 1–24, http://dx.doi.org/10.1080/19401493.2023.2250521, URL https://www.tandfonline.com/doi/full/10.1080/19401493.2023.2250521.

[48] F. Wüllhorst, D. Jansen, P. Mehrfeld, D. Müller, A modular model of reversible heat pumps and chillers for system applications, in: Proceedings of the 14th International Modelica Conference, Linköping, Schweden, 2021, pp. 561–568, http://dx.doi.org/10.3384/ecp21181561, URL https://ecp.ep.liu.se/index.php/modelica/article/view/234.

[49] C. Vering, S. Göbel, T. Klebig, F. Will, J. Horst, F. Wüllhorst, M. Nürenberg, P. Mehrfeld, D. Müller, Towards a defossilized building sector with field tests in the lab: Review, development, and evaluation, Appl. Energy 365 (2024) 123225, http://dx.doi.org/10.1016/j.apenergy.2024.123225, URL https://www.sciencedirect.com/science/article/pii/S0306261924006081.

[50] D.I. für Normung, DIN EN ISO 3743-2:2022-11 - Acoustics - Determination of sound power levels of noise sources using sound pressure - Engineering methods for small, movable sources in reverberant fields - Part 2: Methods for special reverberation test rooms (ISO 3743-2:2018), 2022, URL https://www.dinmedia.de/de/norm/din-en-iso-3743-2/314334164.

[51] D.I. für Normung, DIN EN 15450:2007, Heizungsanlagen in Gebäuden – Planung von Heizungsanlagen mit Wärmepumpen; Deutsche Fassung EN 15450:2007, 2007, URL https://www.beuth.de/de/norm/din-en-15450/98862901.

[52] B. für Wirtschaft und Ausfuhrkontrolle (BAFA), Allgemeines Merkblatt: MAP-Antragstellung in Fragen und Antworten, Tech. rep., Leitungsstab Presse- und Öffentlichkeitsarbeit, Eschborn, 2019.

[53] T. Loga, N. Diefenbach, J. Knissel, R. Born, Entwicklung Eines Vereinfachten, Statistisch Abgesicherten Verfahrens zur Erhebung von Gebäudedaten für die Erstellung des Energieprofils von Gebäuden, Forschungsbericht, INSTITUT WOHNEN UND UMWELT GMBH, Darmstadt, 2005, URL https://www.iwu.de/fileadmin/publikationen/energie/werkzeuge/2005_IWU_LogaEtAl_Kurzverfahren-Energieprofil.pdf.

[54] D. Wetterdienst, S.-u.R. Bundesinstitut für Bau, Ortsgenaue Testreferenzjahre von Deutschland für mittlere, extreme und zukünftige Witterungsverhältnisse, 2017.

[55] P. Stoffel, M. Berktold, D. Müller, Real-life data-driven model predictive control for building energy systems comparing different machine learning models, Energy Build. 305 (2024) 113895, http://dx.doi.org/10.1016/j.enbuild.2024.113895, URL https://www.sciencedirect.com/science/article/pii/S0378778824000112.

[56] T. Blockwitz, M. Otter, J. Akesson, M. Arnold, C. Clauss, H. Elmqvist, M. Friedrich, A. Junghanns, J. Mauss, D. Neumerkel, H. Olsson, A. Viel, Functional mockup interface 2.0: The Standard for Tool independent Exchange of Simulation Models, in: Proceedings of the 9th International MODELICA Conference, München, 2012, pp. 173–184, http://dx.doi.org/10.3384/ecp12076173, URL https://ep.liu.se/en/conference-article.aspx?series=ecp&issue=76&Article_No=17.

[57] D.I. für Normung, DIN ISO 9613-2:1996, Dämpfung des Schalls bei der Ausbreitung im Freien - Teil 2: Allgemeines Berechnungsverfahren, 1999, URL https://nautos.de/7TE/search/item-detail/DE45851807.

[58] I.O. für Normung, ISO 9613-1:1993(e), Acoustics - Attenuation of sound during propagation outdoors - Part 1: Calculation of the absorption of sound by the atmosphere, 1993, URL https://nautos.de/7TE/search/item-detail/IX18942927.

[59] U.u.V.N.W. Landesamt für Natur, Sechste Allgemeine Verwaltungsvorschrift zum Bundes- Immissionsschutzgesetz - Technische Anleitung zum Schutz gegen Lärm, 2017, p. 18, URL https://igsvtu.lanuv.nrw.de/vtu/doc.app?P_VTU_SYSID=002-31&DATEI=6/dokus/62001.pdf.

[60] B.W.B. e.V., Schallrechner, 2019, URL https://www.waermepumpe.de/schallrechner/.

[61] P. Perrin, Simulationsbasierte Analyse der Einflussfaktoren auf Betriebszahlen von Wärmepumpenanlagen (Ph.D. thesis), Technische Universität Carolo-Wilhelmina zu Braunschweig, Braunschweig, 2012.

[62] J. Drgoňa, J. Arroyo, I. Cupeiro Figueroa, D. Blum, K. Arendt, D. Kim, E.P. Ollé, J. Oravec, M. Wetter, D.L. Vrabie, L. Helsen, All you need to know about model predictive control for buildings, Annu. Rev. Control. 50 (2020) 190–232, http://dx.doi.org/10.1016/j.arcontrol.2020.09.001, URL https://linkinghub.elsevier.com/retrieve/pii/S1367578820300584.

[63] M. Bird, C. Daveau, E. O'Dwyer, S. Acha, N. Shah, Real-world implementation and cost of a cloud-based MPC retrofit for HVAC control systems in commercial buildings, Energy Build. 270 (2022) 112269, http://dx.doi.org/10.1016/j.enbuild.2022.112269, URL https://linkinghub.elsevier.com/retrieve/pii/S0378778822004406.

[64] A. Kümpel, T. Storek, M. Baranski, M. Schumacher, D. Müller, A cloud-based operation optimization of building energy systems using a hierarchical multi-agent control, J. Phys.: Conf. Ser. 1343 (2019) 012053, http://dx.doi.org/10.1088/1742-6596/1343/1/012053, 0 citations (Crossref) [2021-03-08]. URL https://iopscience.iop.org/article/10.1088/1742-6596/1343/1/012053.

[65] M. Renner, Akustik in der Lüftungs- und Klimatechnik für die TGA, VDE Verlag GmbH und cci Dialog GmbH, Berlin Offenbach, 2017.

[66] L. Stürenburg, H. Braren, L. Aspöch, J. Fels, Loudness and preference judgments for noises of a heat pump, INTER-NOISE NOISE-CON Congr. Conf. Proc. 270 (6) (2024-10-04) 5415–5423, http://dx.doi.org/10.3397/IN_2024_3589, URL https://www.ingentaconnect.com/content/10.3397/IN_2024_3589.

[67] D.I. für Normung, DIN/TS 12831-1:2020-04, Verfahren zur Berechnung der Raumheizlast - Teil 1: Nationale Ergänzungen zur DIN EN 12831-1, 2020, URL https://nautos.de/7TE/search/item-detail/DE30084519.